Chapter.1. Introduction.

1-1. Background

Advance in semiconductor technology has made rapid progress. And most of the equipments or systems in human society are almost impossible to be improved without semiconductors.

When semiconductor components were developed for the first time, they were demanded only to act like valves. But as the time passed, the demand from the society made the technology of semiconductor raise to the integration. The most developed semiconductor is Si, and which is considered as an undisputed standard in the industry. Si is a very stable material and is also a mature material in the area of crystal growth technology and fine processing technology. And in addition to the properties of Si itself, Si can get a very good insulator (SiO2) on the surface easily. High quality insulator is necessary to fabricate large scale integration circuits (LSI).

But, recently Si has found limited application in new devices such as ultrafast modulators or ultra high density information processing devices. By the other hand, GaAs is the most mature compound semiconductor. In room temperature, the electron mobility of GaAs is about 5 times greater than that of Si. And GaAs can be applied to the optical information processing because GaAs is a direct transition

type semiconductor. But still now, GaAs has not replaced Si. GaAs component is superior to Si's in some aspects, but is not good for the integration.

Some problems have been tried to be solved through advances in crystal growth and processing technology. Integration with a different kind of semiconductor will be the better solution, such as GaAs on Si for example. If it is possible to make LSI using such technique, the limitation in Si technology will be broken through.

The largest advantage of GaAs on Si is the possibility of monolithic integration of both components. The electrical controls are done by the Si and optical controls by the GaAs. Besides that, the advantages of GaAs using Si substrate are:

1.Si substrate is much cheaper than that of GaAs.

2.Si is mechanically strong.

3.larger diameter wafer can easily be obtained (suitable for mass production).

4.Si have larger thermal conductivity. etc.

The crystal growth of GaAs on Si was mainly reported by the use of metal organic chemical vapor deposition (MOCVD), molecular beam epitaxy (MBE), liquid phase epitaxy (LPE) and migration enhanced epitaxy (MEE). But there are common problems to make high quality crystal, which originates from the difference of physical properties between Si and GaAs as follow:

1.Anti-phase domains generates due to a polar semiconductor

on a non-polar semiconductor growth.

2.High density of dislocations generates due to 4.1% lattice mismatch.

3.Stress at room temperature exists due to 62% mismatch in thermal expansion. etc.

These problems make the device application difficult, and they are the largest problems to be solved. Table.1-1. shows the properties of both Si and GaAs.

1-2.Epitaxial growth of GaAs on Si

Numerous investigations for the heteroepitaxial growth of GaAs on Si substrate has been done lately. The purposes of the researches are mainly to reduce the dislocations and to minimize the biaxial tensile stress in GaAs epi-layer. Reduction of dislocations and stress is very important, since dislocations are said to act as a non-radiative recombination center and to produce dark-line defects which degrade the optical device[1][2]. And the stress sometimes produce the dislocations.

The most popular technology of growing GaAs on Si substrate is the two-step method[3~4]. In this method, high electron mobility of $5200cm^2/vs$ and low etch pit density less than $3000cm^{-2}$ can be easily obtained. But the problems about the dislocation and stress are exist by this method.

To reduce the dislocations, many epitaxial methods have been reported. They use a strained-layer supperlattice[5]~[9] as an

Table.1-1. properties of Si , GaAs and AlAs

		Si	GaAs	AlAs
Crystal structure		Diamond	Zincblend	Zincblend
Lattice constant (Å)		5.431	5.653	5.661
Bandgap energy (eV)	300 K	1.12	1.42	3.03
	0 K		1.52	3.13
Electron affinity (eV)	300 K	4.01	4.07	3.5
Crystal density (g/cm^3)		2.329	5.360	3.760
Mobility (m^2/Vs)	electron (300 K)	0.135	0.86	
	hole (300 K)	0.048	0.040	
Thermal expansion coefficent ($\times 10^{-6}$/°C)		2.33	6.4	5.2
Thermal conductivity (W/cmK)	300 K	1.5	0.54	0.08
Dopants	acceptor	B,Al,Ga	Zn,Cd,Ge	
	doner	P,As,Sb	Si,Ge,Sn,Te	

intermediate layer, thermal cycle annealing[10]~[12] and combinations of these techniques[13][14], etc.. However, none of them has successfully reduced the dislocation density to less than 1×10^4 cm^{-2}. And in most of the cases, reducing the dislocations gives rise to make many microcracks.

To minimize the stress is a fundamental and very difficult problem. Because the growth of GaAs requires high temperature, and lowering it to the room temperature after growth raises the stress or bowing. Selective area growth have been proposed to minimize the stress[16]~[21], but only a region of 10μm from the edge allows to reduce the stress and dislocation[19].

Recently, Sakai et al. proposed the so called "Under Cut GaAs on Si" (UCGAS)[22]~[24]. By this method, stress free GaAs layer is reported with no dislocations found in UCGAS layer after annealing at 800°C for 10 minutes. The cross sectional TEM image of UCGAS is shown in Fig.1-1. But in this structure, it is very difficult to fabricate a device. And also the problem about the heat sink arise.

Umeno et al. proposed the irradiation of Yttrium Aluminum Garnet (YAG) laser pulse to the Ge intermediate layer to release the stress in GaAs layer[25]. Five shots of laser pulse irradiation (pulse width was 2ns and its energy was 0.36J/pulse) make the residual stress in GaAs on Si almost to zero, but this method cannot be applied to a larger area.

Research for the high quality GaAs on Si has been done,

Top GaAs

Etched region

Buffer GaAs

1.0μm
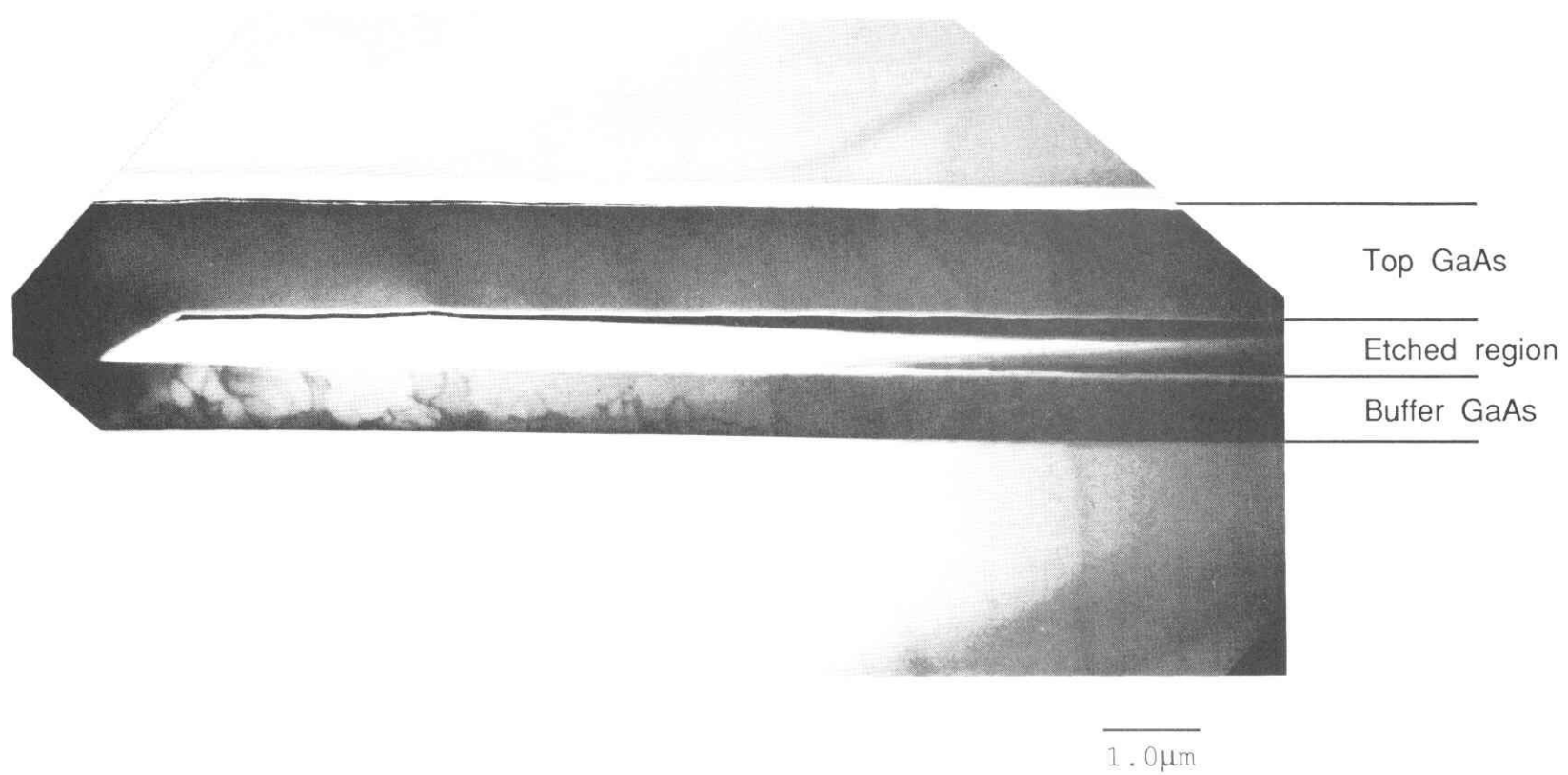
Fig.1-1. The crosssectional TEM image of UCGAS.

There are very little dislocations in the top GaAs layer.

but still now, the most suitable technology has not been founded.

1-3.Application to the devices

The GaAs on Si device of most interest is the optical input/modulate/output one, which can treat the optical information. For this application, many kinds of optical components of GaAs on Si have been reported[26]~[33]. Among them, laser diodes are very popular. T.H.Windhorn et al. have reported the room temperature operation for the first time by MBE growth[34]. In the case of MOCVD, which has advantages in mass production, Sakai et al. have reported the use of a strained layer supperlattice as an intermediate layer[35][36].

The first report of room-temperature continuous wave (cw) operation was done by Deppe et al. using AlGaAs/GaAs quantum well (QW) heterostructure[37][38]. In their report, the growth of the buffer layer was done by MBE method and the laser structure by MOCVD. Choi et al[39]. and Egawa et al. have reported a room-temperature cw operation by all-MOCVD-growth laser technology using thermal cycle annealing to reduce dislocations[40]. But the problem about lifetime, which is the most serious and difficult problem for lasers, still remains. At the present, the lifetime of GaAs and AlGaAs laser does not exceeds one hour. For GaAs, AlGaAs and InGaAs laser 56 hours[41], and InP more than 1000 hours[42].

Application to solar cells are also reported. Yamaguchi et al. have fabricated high efficiency solar cell with total efficiencies of 18.3% (AM0) and 20% (AM1.5)[43]. Shimizu et al. reported tandem sollar cell of 32% efficiency in theory[44], but the experimental result showed just 16.3%. One of the reasons of this result was the degradation of the photocurrent at the region of Si interface in GaAs layer.

Kim et al. have reported a phase modulator[45], with an average TE mode propagation loss of 1.24 dB/cm in 6μm width ridge waveguide and phase shift efficiency of 3.5°/Vmm (it is about 3 times larger than that of GaAs substrate) at a λ=1.3μm wavelength. G.V.Treyz et al. reported a multiple quantum well (MQW) waveguide switch fabricated by MBE. This was a slab-type waveguide and shows 20dB/cm modulation at λ=900nm for a reverse bias of 2.5V[46].

Besides, MESFET[47][48] and HEMT[49] on Si substrate are proposed. The difficulties of these devices are mainly the control of the carrier concentration and the control of the resistivity of the epi-layer. GaAs on Si is sometimes affected by the Si-autodoping from Si substrate. Si in GaAs act as a n-type dopant, so how to avoid such an effect is an important problem.

Thus, there are many approaches for the GaAs on Si device. The disturbing factors to the device applications are stress, dislocations and impurity autodoping, which commonly affects the device properties. Especially, these factors affect strongly active devices such as laser or LED

where much power is needed. But with the progress of the epitaxial growth technology and improvement of the quality of epi-layer, these problems have been gradually come to an end.

1-4.The purpose and organization of this dissertation

Recently, the technology for making of GaAs devices has been advanced, and in future, high speed signal processing (such as optical computing or board to board optical communications) will be performed by the integration. For them, optoelectronic integrated circuits (OEIC's) will be needed. Such an integration of all optoelectronic components in one chip requires the development of the optical waveguide, optical modulators and optical switches as an interconnection between active devices. Recently optical device applications utilizing the quantum well properties (such as room temperture exciton effect etc) are very popular and many device applications have been reported. The reserches about the devices application of the QWs tends to increase and this tendency will make all semiconductor OEIC applications easier.

The research of GaAs on Si, which has given considerable attention for OEIC's, also needs to aim for the application in optical interconnections. The purpose of this dissertation is the application of GaAs on Si to the optical waveguide and concerning devices.

This dissertation is composed of 6 chapters, each one of them summarized below.

Chapter 1. is the introduction of this dissertation and describes the development of the crystal growth of GaAs on Si and the applications to devices.

In chapter 2., the applications to the optical waveguide of GaAs on Si are described. Three-dimensional DH-type waveguides were designed and near field patterns were observed.

In chapter 3., the quantum well properties are described. The calculation results of the GaAs quantum level in Al0.25Ga0.75As on Si are shown. And the measured value of the quantum level by photocurrent or photoluminescence is compared with the calculated one. Then QCSE in GaAs QW on Si is evaluated.

In chapter 4., applications to the optical switch are described. QCSE of the SQW fabricated in the core layer of the waveguide on Si are applied to the switch. The switching properties are shown. The application to the 850nm optical switch and the possibility to be integrated with the laser diode are also discussed.

In chapter 5., applications to the phase modulator are described.

Chapter 6. is the summary of this dissertation, and a scope for future work is also given.

References

1) A.S.Jordan, A.R.von Neida and R.J.Matyi:Appl.phys.Lett.,
   50,(1987)992.

2) M.Yamaguchi and S,Kondo:Mater.Res.Soc.Symp.Proc.,145,
   (1989)279.

3) M.Yamaguchi,T.Nishioka and M.Sogo:Appl.Phys.Lett.,54,
   (1989)24.

4) M.Akiyama,Y.Kawarada and K.Kaminishi:Jpn.J.Appl.Phys.,
   23,(1984)L843.

5) R.Fischer,D.Neuman,H.Zabel,H.Morkoc,C.Choi and N,Otsuka:
   Appl.Phys.Lett.,48,(1986)1223.

6) T.Soga,T.Imori and M.Umeno:Mater.Res.Soc.Symp.Proc.,91,
   (1987)69.

7) N.El-Masry,N.Hamaguchi,J.C.L.Tarn,N.Karam,T.P.Humphreys,
   D.Moore and S.M.Bedair:Mater.Res.Soc.Symp.Proc.,91,
   (1987)99.

8) N.Hayafuji,S.Ochi,M.Miyashita,M.Tsugami,T.Murotani and A.
   Kawaguchi:J.Cryst.Growth,93,(1988)494.

9) T.Soga,T.Jimbo,and M.Umeno:Appl.Phys.Lett.,56,(1990)1433.

10) J.W.Lee,H.Shichijo,H.L.Tsai and R.J.Matyi:Appl.Phys.
    Lett.,50,(1987)31.

11) C.Choi,N.Otsuka,G.Munns,R.Houdre,H.Morkoc,S.L.Zhang,D.
    Levi and M.V.Klein:Appl.Phys.Lett.,50,(1987)992.

12) A.Freundlich,J.C.Grenet,G.Neu,A.Leycuras and C.Verie:
    Appl.Phys.Lett.,52,(1988)1976.

13) M.Yamaguchi,A.Yamamoto,M.Tachikawa,Y.Itoh and M.Sugo:

Appl.Phys.Lett.,53,(1988)2293.

14) M.Akiyama,Y.Kawarada and K.Kaminishi:J.Cryst.Growth,68, (1984)21.

15) S.Nishi,M.Akiyama,and K.Kaminishi:Extended Abstruct of the 17thConference on SSDM Tokyo,Japan(1985)213.

16) M.Yamaguchi,M.Tachikawa,M.Sogo and S.Kondo:Appl.Phys. Lett.,56,(1990)27.

17) N.Chand,J.P.von der Ziel,J.S.Weiner,A.M.Sergent and A.Y. Cho:Appl.Phys.Lett.,53,(1988)225.

18) B.G.Yacobi,C.Jagganath,S.Zemon and P.Sheldon:Appl.Phys. Lett.,53,(1988)555.

19) H.P.Lee,S.Wang,Y.H.Huang and P.Yu:Appl.Phys.Lett.,52, (1988)215.

20) R.J.Matyi,H.Shichijo,T.H.Moore and H.L.Tai:Appl.Phys. Lett.,51,(1987)18.

21) P.Sheldon,K.M.Jones,R.E.Hayes,B.Y.Tsaur and J.C.C.Fan: Appl.Phys.Lett.,45,(1984)274.

22) S.Sakai,K.Kawasaki and N.Wada:Jpn.J.Appl.Phys.,29,(1990) L853.

23) S.Sakai,C.L.Chao,N.Wada,T.Yuasa and M.Umeno:Appl.Phys. Lett.,66,(1992)1480.

24) N.Wada, S.Yoshimi, S.Sakai, C.L.Chao and M.Fukui:Jpn.J. Appl.Phys.,31,(1992)L78.

25) M.Umeno,T.Soga and T.Jimbo:Jpn.J.Appl.Phys.,31,(1992) 1189.

26) S.Sakai,T.Soga,M.Takeyasu and M.Umeno:Jpn.J.Appl.Phys., 24,(1985)L666.

27) S.Sakai,H.Shiraishi and M.Umeno:IEEE Ouantum Electron., QE-23, (1987)1080.

28) R.W.Kaliski,N.Holonyak,Jr.,K.C.Hsieh,D.W.Nam,J.W.Lee,H. Shichijo,R.D.Burnham,J.E.Epler and H.F.Chung:Appl.Phys. Lett.,50, (1987)836.

29) T.C.Chong and C.G.Fonstad:Appl.Phys.Lett.,51, (1987)221.

30) D.G.Deppe,D.W.Nam,N.Holonyak,Jr.,K.C.Hsieh,R.J.Matyi,H. Shichijo,J.E.Epler and H.F.Chung:Appl.Phys.Lett.,51, (1987)1271.

31) T.Egawa,Y.Kobayashi,Y.Hayashi,T.Soga,T.Jimbo and M. Umeno:Jpn.J.Appl.Phys.,29, (1990)L1133.

32) Y.S.Kim,S.S.Lee,R.V.Ramaswamy and S.Sakai:Appl.Phys. Lett.,56, (1990)802.

33) T.Yuasa,M.Umeno,S.Sakai,N.Wada and Y.Ueta:Mater.Res.Soc. Symp.Proc.,228, (1992)225.

34) T.H.Windhorn and G.M.Metze:Appl.Phys.Lett.,47(1985)1031.

35) S.Sakai,T.Soga,M.Takeyasu and M.Umeno:Appl.Phys.Lett., 48, (1986)413.

36) S.Sakai,H.Shiraishi and M.Umeno:IEEE Quuantum Electron., QE-23, (1987)1080.

37) D.G.Deppe,N.Holonyak,Jr.,D.W.Nam,K.C.Hsieh,R.J.Matyi,H. Shichijo,J.E.Epler and H.F.Chung:Appl.Phys.Lett.,51, (1987)637.

38) D.G.Deppe,D.N.Nam,N.Holonyak,Jr.,K.C.Hsieh,R.J.Matyi,H. Shichijo,J.E.Epler and H.F.Chung:Appl.Phys.Lett.,51, (1987)1271.

39) H.K.Choi,C.A.Wang and J.C.C.Fan:J.Appl.Phys.,68, (1990)

1916.

40) T.Egawa,H.Tada,Y.Kobayashi,T.Jimbo and M.Umeno:Appl.
Phys.Lett.,57, (1990)1179.

41) H.K.Choi, C.A.Wang and N.H.Karam:Appl.Phys.Lett.,59,
(1991)2634.

42) M.Sugo, H.Mori, Y.Sakai and Y.Itoh:Appl.Phys.Lett.,60,
(1992)472.

43) M.Yamaguchi and S,Kondo:Mater.Res.Soc.Symp.Proc.,145,
(1989)279.

44) H.Shimizu,T.Egawa,T.Soga,,T.Jimbo and M.Umeno:Jpn.J.
Appl.Phys.,31, (1992)L1150.

45) Y.S.Kim,S.S.Lee,R.V.Ramaswamy,S.Sakai,Y.C.Kao and H.
Shichijo:Appl.Phys.Lett.,56, (1990)802.

46) G.V.Trey,P.G.May,D.Latulipe,S.Basu and W.I.Wang:Appl.
Phys.Lett.,57, (1990)1078.

47) H.K.Choi,B.Y.Tsaur,G.H.Matze,G.W.Turner and J.C.C.Fan:
IEEE Electron.Device Lett.,EDL-5, (1984)207.

48) T.Nonaka,M.Akiyama,Y.Kawarada and K.Kaminishi:Jpn.J.
Appl.Phys.23, (1984)L919.

49) R.Fisher,M.Kopp,J.S.Gedymin and H.Morkoc:IEEE Electron.
Device,ED-33, (1986)1407.

Chapter 2. Properties of the waveguide of GaAs on Si.

2-1.Introduction

One important reason of growing GaAs on Si substrate is to make OEIC's combining GaAs optical components and Si electrical components. For this purpose, optical components for the integration (such as waveguide, coupler and modulator etc.) are essential. Especially, the optical waveguide is the most fundamental and the most important component. If the purpose of GaAs on Si is aiming for the integration, it is necessary to investigate the properties of the optical waveguide fabricated on Si substrate. GaAs grown on Si substrate has a lot of dislocations and stress, and the surface morphology of GaAs grown by MOCVD is not flat enough (see Fig.2-1), so it gains a lot of interest to investigate how these undesired properties affects the optical waveguide. But still now, the results obtained about them are very few.

In this chapter, we show the properties of an optical waveguide fabricated on Si substrate. The prepared samples were Al0.1Ga0.9As/GaAs/Al0.1Ga0.9As DH-type optical waveguides in different structures. We evaluated the effects from the dislocations or other factors by measuring the near field patterns and their intensity profiles.

2-2.Sample preparation
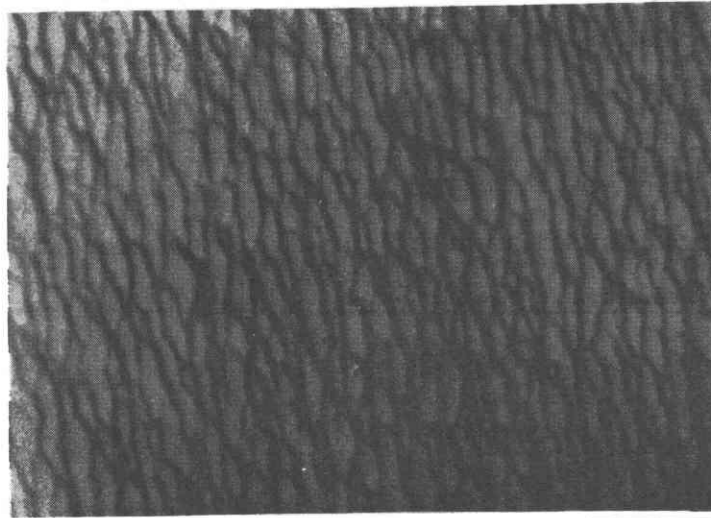
10μm

Fig.2-1. The surface morhology of the GaAs grown by MOCVD.

There are macrosteps at the surface. Their intervals are 2~7μm long and step-height was about 10~20nm.

Table.2-1.The epitaxial conditions of the sample shown in Fig.2-1.

used substrate	: n-Si 2° off toward [011]
initial growth metod	: two-step method
growth temperature	: 750°C
growth rate	: 3.0μm per hour
thickness of the sample	: 3.0μm

2-2-1. Design of the waveguide

The double-heterostructure(DH) waveguide of fundamental mode in both vertical (parallel to the growth direction) and horizontal (parallel to the propagation direction) is designed by the effective index method[1]. The schematic model for analysis is shown in Fig.2-2. The thickness of both cladding layers (top and bottom) are 1μm. The effective index in region I and III are related to the propagation constant β which can be calculated from the four-layer slab waveguide (ie. air, thin top cladding layer, guiding layer and bottom cladding layer). The equations used for the calculation are shown below[2]:

$$N=\beta/k \qquad\qquad 2\text{-}1.$$

$$k=2\pi/\lambda \quad (\lambda:\text{wavelength}) \qquad\qquad 2\text{-}2.$$

The propagation constant β is obtained by solving the eigenfunction:

$$\tan(h\ d) = \frac{p + q + (p - q)\ V}{h - pq\ /\ h + (h + pq\ /h)\ V}$$

$$\text{here} \quad V = \frac{(q - r)}{(q + r)}\ \exp(-2qt) \qquad\qquad 2\text{-}3.$$

$$p=(\beta^2-n_1^2k^2)^{1/2} \quad , h=(n_2^2k^2-\beta^2)^{1/2} \qquad 2\text{-}4.$$

$$q=(\beta^2-n_3^2k^2)^{1/2} \quad , r=(\beta^2-n_4^2k^2)^{1/2}$$

And the electric field components (E_y) are assumed to be:

$$E_y= \ A\ \exp(px) \qquad\qquad :(x\leq0) \qquad 2\text{-}5.$$

w

x=d+t

x=d

Region I | Region II | Region III

x=0

Top Cladding Layer
($Al_{0.1}Ga_{0.9}As$)

Guiding Layer
(GaAs)

Bottom Cladding Layer
($Al_{0.1}Ga_{0.9}As$)

Si substrate
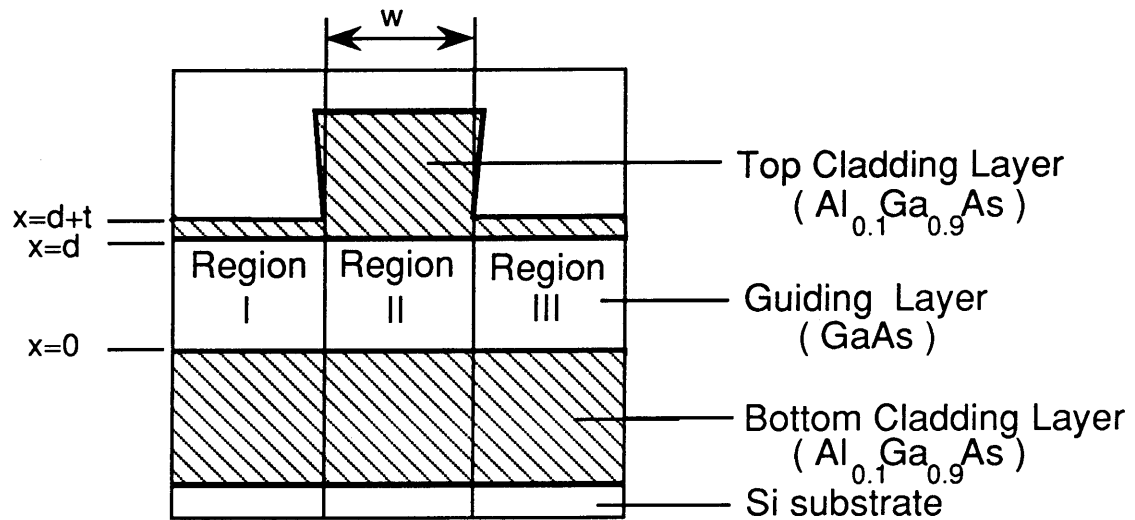
Fig.2-2. The schematic model for analysis.

- Effective refractive index in region I, III were calculated from four layers' refractive indexes of Air, Al0.1Ga0.9As, GaAs and Al0.1Ga0.9As.

- Effective refractive index in region II was calculated from three layers' refractive indexes of Al0.1Ga0.9As, GaAs and Al0.1Ga0.9As.

$$B \exp(ihx) + C \exp(ihx) \qquad : (0 \leq x \leq d)$$

$$D \exp[-q(x-d)] + E \exp[q(x-d)] \quad : (d \leq x \leq d+t)$$

$$F \exp[-r(x-d-t)] \qquad : (x \geq d+t)$$

here A-F are the amplitude coefficients and n_j (j=1~3) are the refractive indexes of the epitaxial layer and n_4 is that of air (n_4=1). The Si substrate effect over the refractive index of the guiding layer can be neglected due to the thickness of the bottom cladding layer. In region II, the effect of the air can also be neglected. The bulks refractive indexes of AlxGa1-xAs[3)4)] were used in this calculation.

The calculated results for the effective refractive index in region II as a function of the thickness of the top cladding layer (t) are shown in Fig.2-3. It also shows the longest ridge width (WLimit) which is the largest value to confine the traveling light as a single mode in the horizontal direction. In the calculation, the thickness of the GaAs guiding layer (d) is 0.7μm and its refractive index is 3.4150, while cladding layer is Al0.1Ga0.9As and its refractive index is 3.3678. The used wavelength for this calculation is 1.3μm.

2-2-2.Sample structure

The structure of waveguide was formed by three layers [Al0.1Ga0.9As (top cladding layer), GaAs (guiding layer) and Al0.1Ga0.9As (bottom cladding layer)]. All the layers were
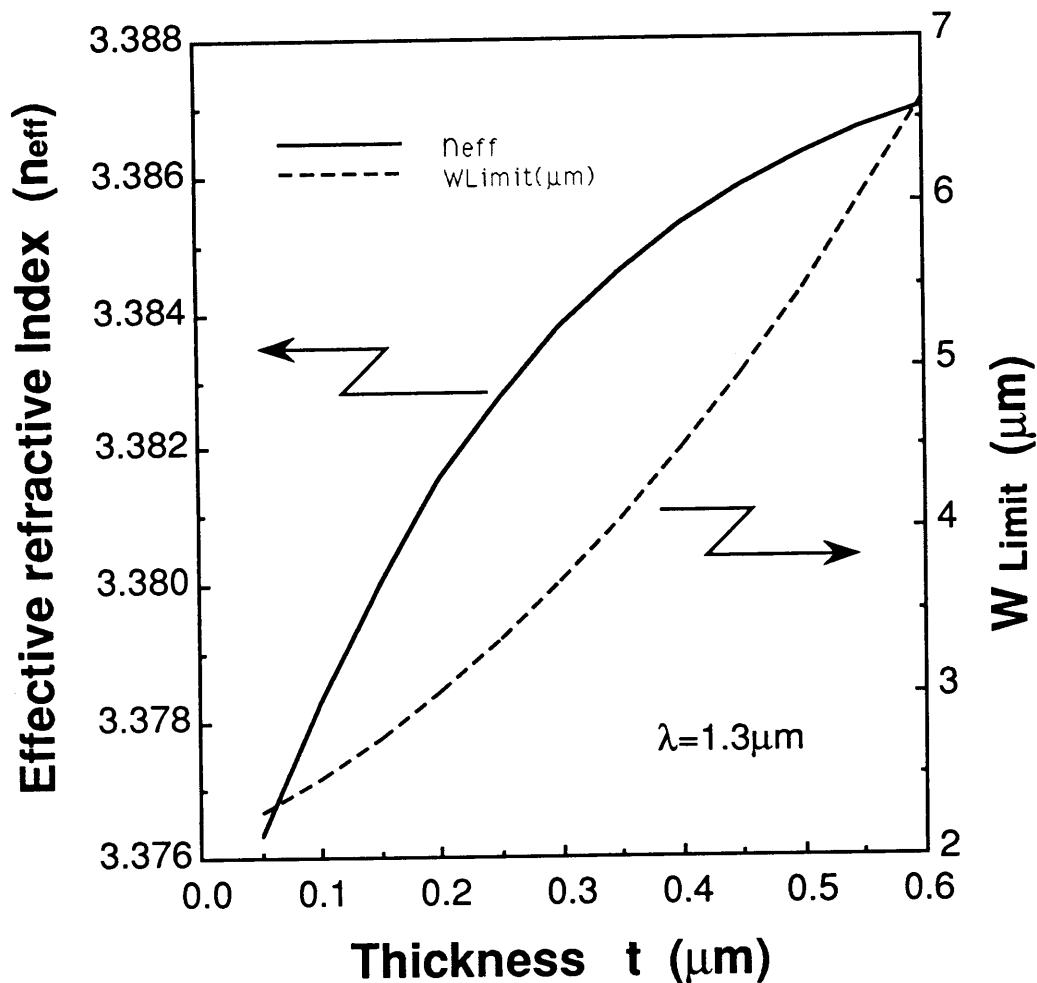
Fig.2-3. The calculated effective refractive index in region II and maximum ridge width (WLimit) to confine as a single mode.

Solid line shows the effective index (neff) of region II as a function of the thickness (t). Dashed line shows the maximum value of the ridge width (W) to confine as a single mode in the vertical (to the growth) direction.

grown by atmospheric MOCVD. TMG and AsH_3 were used for gas source and H_2 as the carrier. A (100) Si oriented 2° off, toward [011] direction was used for the substrate. The back of the Si substrate was coated by SiO_2 (about 0.3μm thick) to avoid Si-autodoping from the back to the surface. The well-known two step method was used. The conduction type of every layer was n-type. The electron concentration in top cladding layer, guiding layer and top region of the bottom cladding layer were found to be less than $1 \times 10^{16} cm^{-3}$ obtained by capacitance-voltage measurement using Polaron's semiconductor profiler. In the bottom cladding layer, the carrier concentration gradually increased from the point of 0.5μm to the Si surface and finally reached more than $1 \times 10^{18} cm^{-3}$ at the interface of Si substrate. The profile of carrier concentration is shown in Fig.2-4. The ridge structure for the waveguide along the [011] direction of Si substrate was fabricated by conventional photolithography and wet chemical etching. The etchant $NH_4OH(28wt\%):H_2O_2$ $(35wt\%):H_2O=20:7:100$ was used. This etchant is known as being an unisotropic etchant for GaAs. The width of the ridge (W) was 2μm, and etched depth was changed by the etching terms. The etching rate of this etchant at 4°C degree is about 1.1μm per minute. The sample's back was polished to about 100μm thick and the waveguide facets were prepared by cleaving. The length of the waveguide was 1~2mm long. The schematic cross-section of the waveguide facet and the picture by SEM are shown in Fig.2-5 and Fig.2-6,

Carrier Concentration (cm^{-3})

10^{19}

Top cladding region | Guiding region | Bottom cladding region | Si

10^{18}

10^{17}

10^{16}

0   1   2   3

Depth (μm)
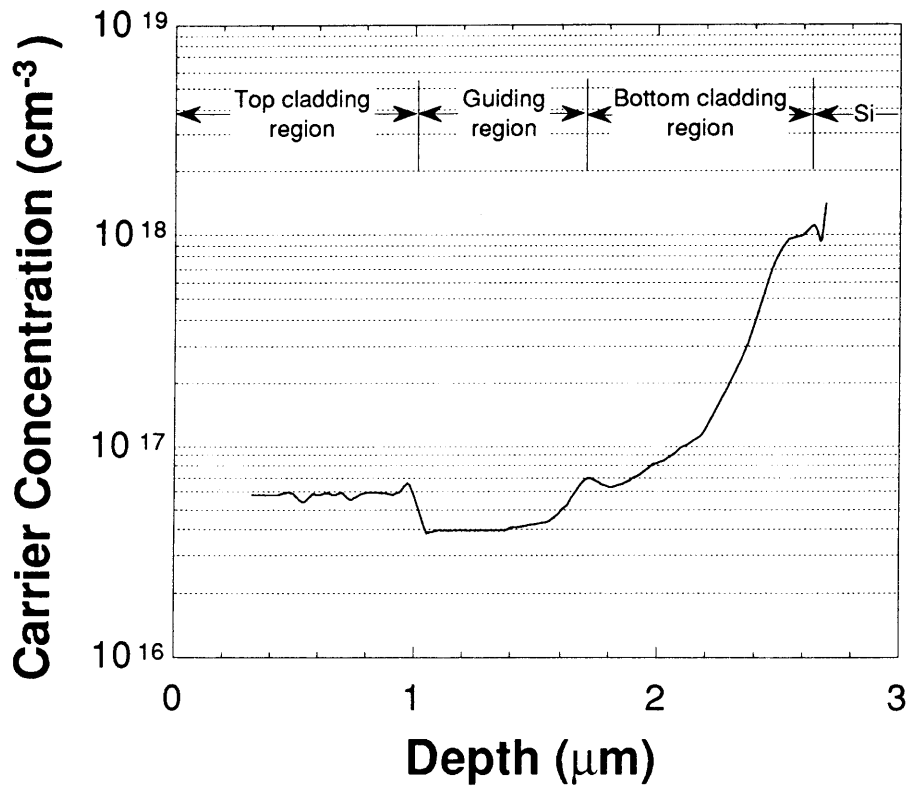
Fig.2-4. The profile of carrier concentration in the waveguide measured by capacitance-voltage measurement.

The conduction type is n-type. The carrier concentration gradually increases from the point of 0.5μm to the Si surface.
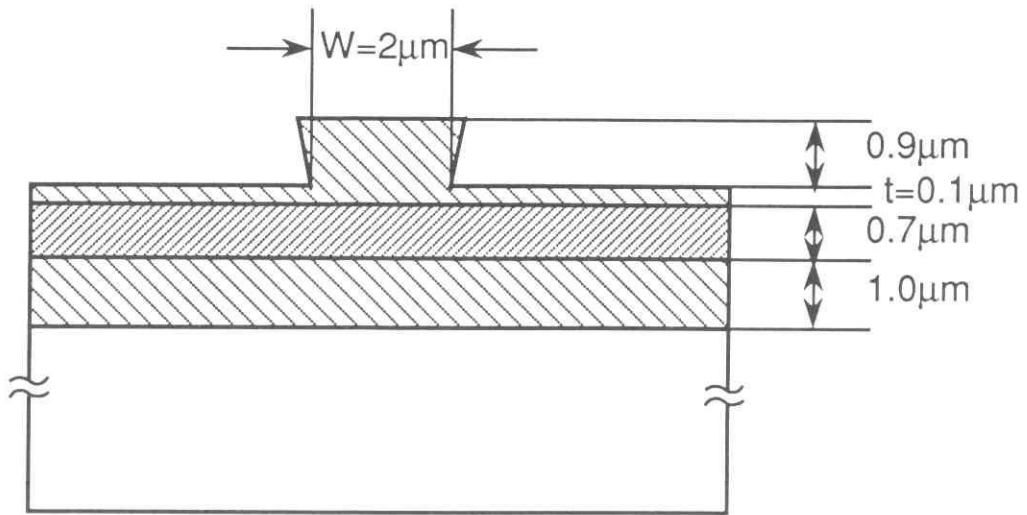
Fig.2-5.The schematic crosssection of the waveguide facet.
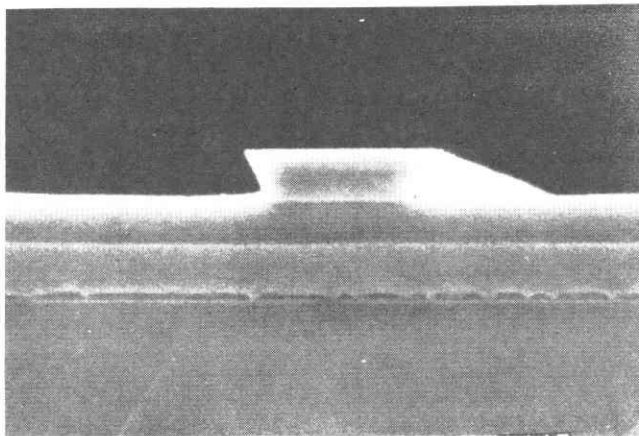
1μm

Fig.2-6. The crosssectional SEM image of the waveguide.

respectively. In this sample, the mesa-height was 0.9μm and ridge width was 2.0μm.

2-3.Near field patterns

2-3-1.Measuring method

The optical properties of the waveguide were evaluated by using distributed feed-back laser diode (DFBLD) of 1.3μm wavelength as a light source. A schematic experimental set up is shown in Fig.2-7. The laser beam was focused into the cleaved facet of a single mode optical fiber. Then the output-beam from the other side of the fiber was directly led into the waveguide facet. Input laser beam polarization was adjusted to TE-mode. A He-Ne laser was used for optical alignment. The near field patterns of the waveguide were focused into an infrared vidicon and displayed on a TV monitor. The near-field intensity profiles were given by an image analyzer.

2-3-2.Near-field patterns of the slab waveguide

The obtained near field pattern of the slab waveguide and the crosssectional SEM image of the measured sample are shown in Fig.2-8. The traveling light can be confined in only a vertical (depth) direction due to the difference of the refractive index between GaAs and Al0.1Ga0.9As. Fig.2-8 b) shows that the traveling light is strongly confined symmetrically in the vertical direction. The intensity
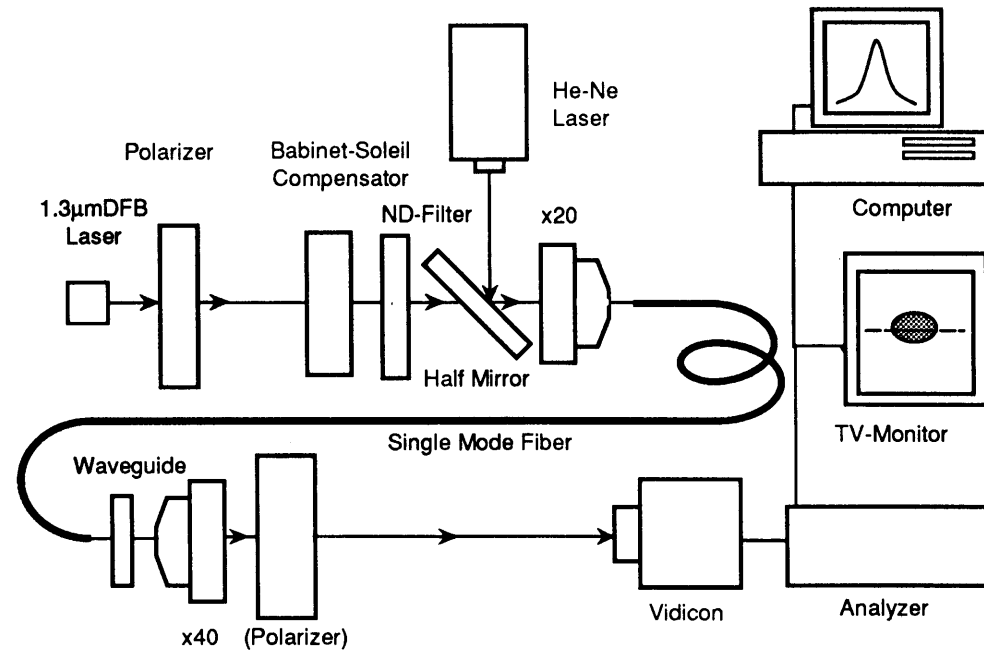
Fig.2-7. Schematic experimental setup to evaluate the near field patterns and the near field intensity profiles.

Cladding Layer
Guiding Layer
Cladding Layer

Si Substrate

1.0μm
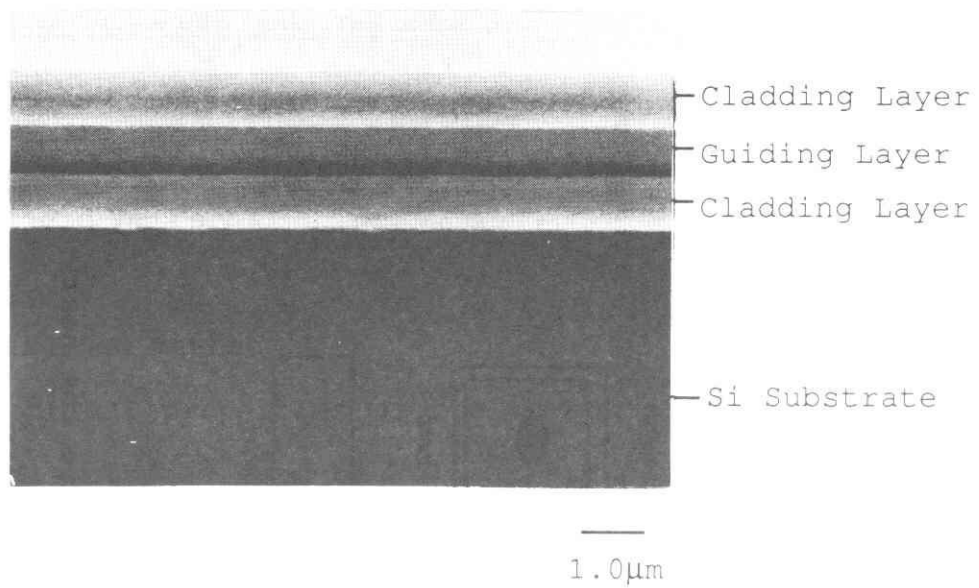
a).The SEM image of the slab waveguide.

VIEW DIRECTION ▼

step=04

5.0μm
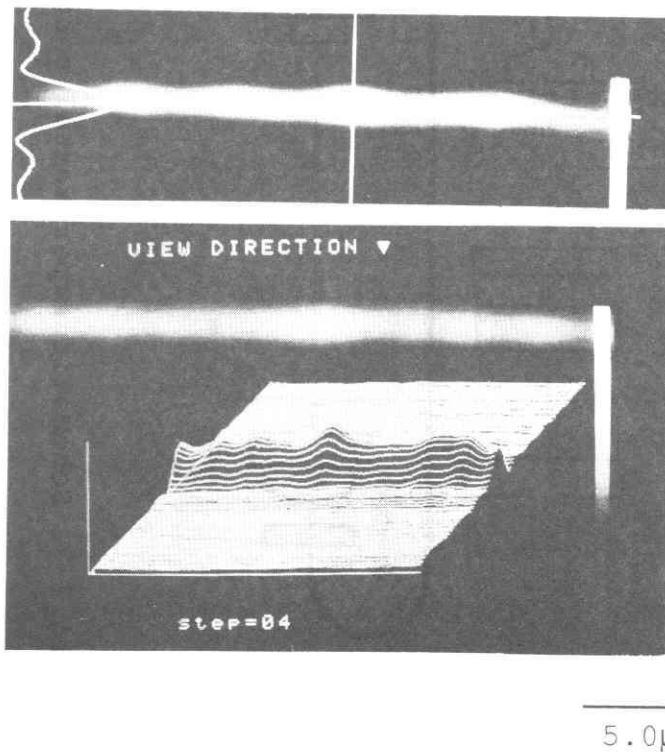
b).The near field pattern and the intensity

profiles in vertical direction (upper), and

3D intensity pattern (lower).

Fig.2-8. The slab waveguide and its near field pattern.

a).SEM image, b).nearfield pattern and its intensity.

profile shows that the high dislocation density does not seem to affect strongly the traveling light. There were more than $1 \times 10^5 cm^{-2}$ dislocations at the surface region of the sample and the number of dislocations tends to increase in the lower region (near the interface with the Si surface, more than $1 \times 10^8 cm^{-2}$ dislocations were counted). If these dislocations affect the refractive index or the absorption rate strongly, the near field intensity profile cannot be symmetrical in the vertical direction.

In the near field pattern, there are some dark spots. This shows that there are some factors which absorb or disturb the traveling light in the crystal. Compared with the dislocation density, the number of dark spots is very small. The origin of the dark spots is not clear, but there are some factors to be considered. They are as follows:

1).Stacking faults: which sometimes occur in the crystal of GaAs on Si and affect a larger area compared with the dislocations.

2).Macrosteps: which are due to the high temperature growth by MOCVD at around 700°C~800°C (see Fig.2-1), and are about $(1\sim5) \times (1\sim5) \mu m^2$ width 100~200Å in height.

As the interval of the dark spots is about 2~5μm, the origin of them seems to be the macrosteps.

2-3-3.Near field patterns of the ridged waveguide

We prepared four-types of ridged waveguide with different etched depths (0.60, 0.70, 0.80,and 0.90μm). The

near field patterns of them are shown in Fig.2-9 and Fig.2-10 shows the 3-dimensional intensity profile in the mesa height 0.90μm. The near field intensity profiles and those calculated from their structures (using the equations 2-1 ~ 2-5) are shown in Fig.2-11.

The near field profiles show that the guides were single mode and were well confined both in vertical (depth) and lateral (width) directions. The intensity profiles show that the measured and calculated profiles agree quite well each other for all the waveguides, which have different mesa heights. In the shallower-ridged waveguide, some satellite peaks appear in the intensity profiles. The origin of these peaks is discussed above. The effects of such factors strongly affect the weakly confined structure (shallower ridged type). But in the strongly confined structure (deep ridged type), the effects from them are considered relatively small enough. Anyway, main profiles observed agree well with the calculated ones for all etched depths. These results mean that it is possible to design AlGaAs/GaAs DH optical waveguides on Si substrate in the same way as we do on the GaAs substrate.

2-4.Propagation loss

It is very important to estimate the propagation loss of the waveguide on Si substrate. One of the reports of DH-type AlGaAs/GaAs stripe roaded waveguide on GaAs substrate
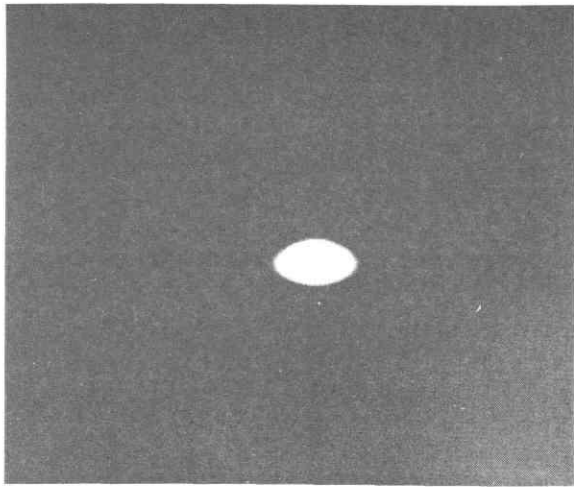
a).t=0.10μm
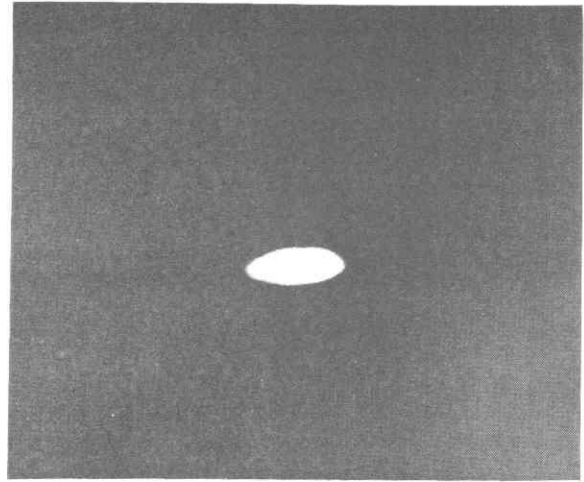
b).t=0.20μm
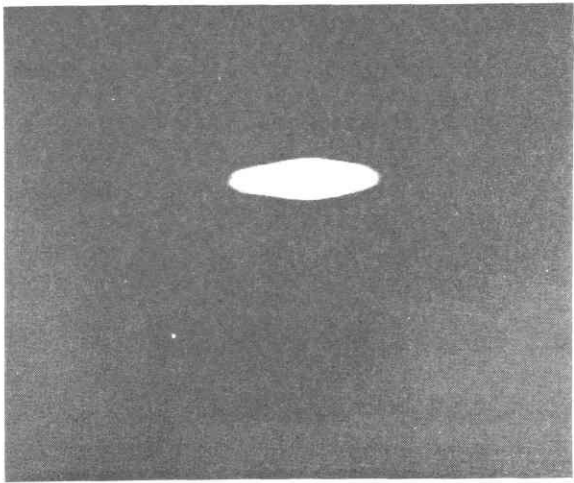
c).t=0.30μm
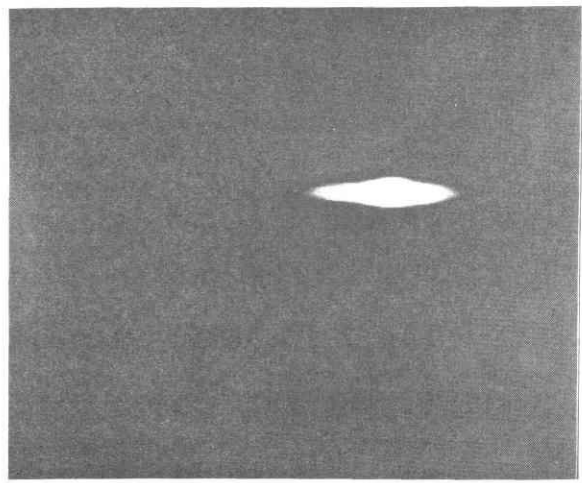
d).t=0.40μm

5.0μm

Fig.2-9. The near field patterns of the ridged
waveguide on different mesa heights.
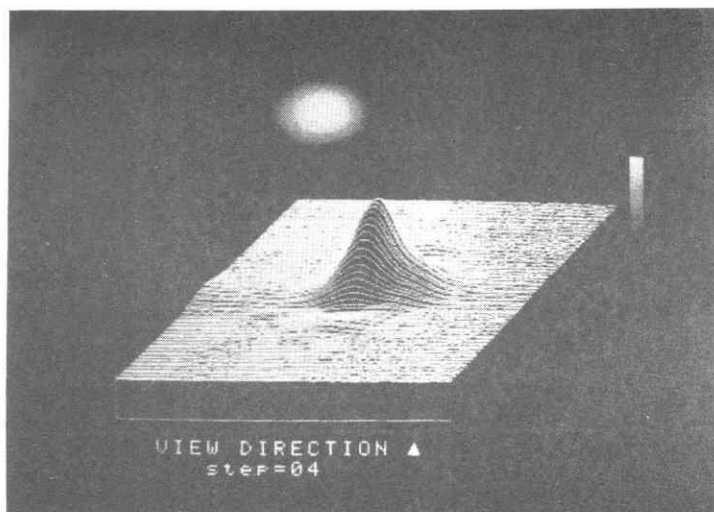
Fig.2-10. Three dimensional intensity profile of the near-field pattern of the waveguide. In this sample, t=0.1μm and W=2.0μm
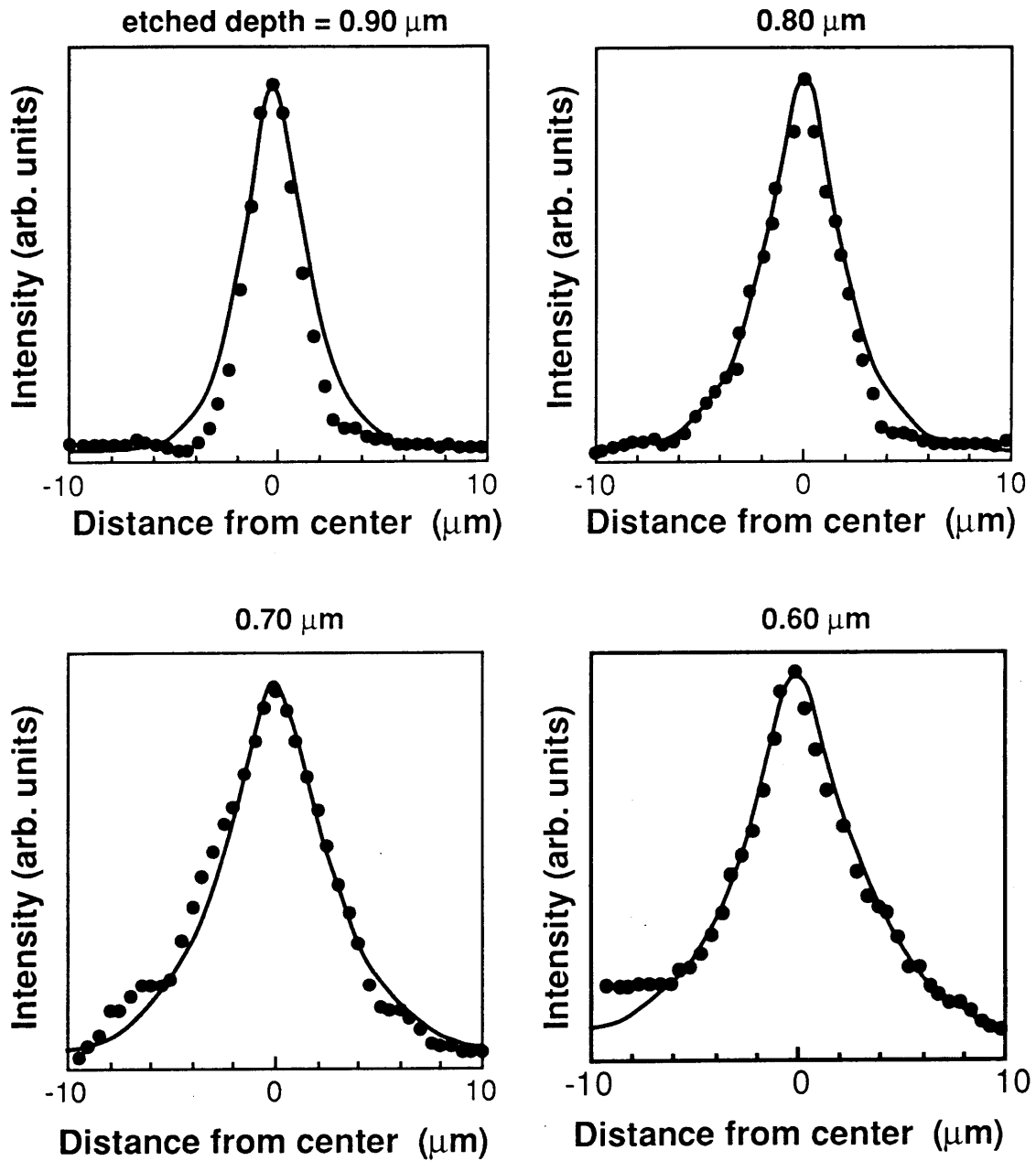
Near field intensity profiles

—— calculated; ● mesured

Fig.2-11. The comparison of the near field intensity profiles and these of the calculated.

grown by MOCVD shows a propagation loss of 2dB/cm and coupling efficiency of 70% at a wavelength λ=1.3μm[6]. In the case of GaAs on Si, 11.2dB/cm was reported[7] in the ridged type waveguide grown by MBE. And the minimum value of the propagation loss at λ=1.3μm was reported to be 1.24dB/cm in the single-mode AlGaAs/GaAs single heterostructure ridged waveguide[8]. This value is extremely small compared with other reports of not only on Si substrate but also on GaAs substrate.

The propagation loss was caused mainly due to the relatively large free-carrier concentration in the guiding layer and also surface and ridge wall scattering, leakage through substrate and absorption loss from interband and height impurity. They depend on the structure (for example, the width and height of the guiding layer) and the quality of the waveguide. The surface morphology of GaAs on Si by MOCVD is not so flat compared with that by MBE. The scattering seems to be larger (estimated to be 2~3dB/cm). In this structure the effect from the carrier concentration (4×10^6) is around 10dB/cm[6]. Considering all those factors the propagation loss is expected to be around 15dB/cm[9][10].

The propagation loss is measured by the conventional cut-back method. The prepared sample is a ridged DH-structure (whose near filed patterns are shown in Fig.2-9) The measured losses were around 20~25dB/cm. These values were greater than we expected but were not a serious problem. Perhaps the scattering was larger than the

expected.

2-5.Conclusion.

The characteristics of GaAs on Si DH optical waveguide were studied. The near field patterns and their intensity profiles were measured at the wavelength of $\lambda=1.3\mu m$. The refractive indexes of AlxGa1-xAs used for this calculation were bulk's ones that ever reported. The obtained profiles agree quite well with these of the calculated ones by the effective index method. This also shows that the refractive indexes of AlxGa1-xAs on Si were very similar to these of the bulk's and can be substituted by them.

In the near field pattern, some dark spots were found. They were 2~7μm intervals and those were almost the same as the intervals of the surface macrosteps. The effects to the near field of the dark spots decrease as the confinement becomes strong. This shows that the effect of the dark spots is not so strong and cause almost no problems to ridged waveguides.

The propagation loss was also estimated. The value of the loss was around 20~25dB/cm. They are mainly due to the free-carrier absorption, and surface and ridge wall scattering. This value is a little larger if compared with the reported value of the one fabricated on a GaAs substrate. The loss will become smaller with advance in crystal growth technology.

Waveguide is the most fundamental and the most important component for the integration. And it is possible to apply to other optical devices such as modulators or switches. In this meaning, the studies in this chapter shows important results.

References

1) R.G.Hunsperger:Integrated Optics;Theory and Technology second edition, Springer-Verlag Berlin Heidelberg, (1984).

2) T.Kuroda, M.Nakamura, K.Aiki and J.Umeda:Applied Optics, 17,(1978),3264.

3) S.Adachi:J.Appl.Phys.,58,(1985),R1.

4) D.E.Aspnes, S.M.Kelso, R.A.Lagon and R.Bhat:J.Appl.Phys., 60,(1986),754.

5) T.Yuasa, M.Umeno, S.Sakai, N.Wada and Y.Ueta:Mat.Res.Soc. Symp.228,(1992),225.

6) S.H.Lin, S.Y.Wang, S.A.Newton and Y.M.Houng:Electron. Lett.,21,(1985),597.

7) Y.S.Kim, S.S.Lee, R.V.Ramaswamy, S.Sakai, R.J.Matyi and H.Shichijo:Appl.Phys.Lett.,53,(1988),1586.

8) Y.S.Kim, S.S.Lee, R.V.Ramaswamy, S.Sakai, Y.C.Kao and H. Shichijo:Appl.Phys.Lett.,56,(1990),802.

9) R.J.Deri, D.E.Kapon and L.M.Schiavone:Electron. Lett.,23, (1987),845.

10) W.G.Spitzer and J.M.Whelan:Phys.Rev.Lett.,114,(1959),59.

Chapter 3. Quantum well properties of GaAs on Si.

3-1.Introduction

Multi-quantum well (MQW) is a peculiar structure of compound semiconductors, and its properties have received much attention recently. That is because the MQW shows some interesting properties. Especially the optical phenomena, which are concerning to the room temperature exciton and can be applied not only for the light emission/absorption devices but also to the new "light control" devices. As for example, optical bistability etalon[1][2], optical modulator[3]~[6] and self-electrooptic effect device (SEED)[7]~[9] etc. are typical ones.

MQW can be easily fabricated by MOCVD only by changing the gas flow ratio of trimethyl Aluminium (TMA) and trimethyl Gallium (TMG)[10].

The purpose of this chapter is to investigate the QW properties of GaAs/AlGaAs on Si fabricated by MOCVD and to make sure if it is possible to apply its property to the QW devices. First, the TEM pictures and Photo-Luminescence (PL) spectra of the GaAs/AlGaAs QW on Si substrate fabricated by MOCVD are shown to evaluate the effect from dislocations. Then, to evaluate the effect from the stress, the calculation results of the absorption energy in $Al_{0.25}Ga_{0.75}As$/GaAs QW in different well widths, with the consideration of the stress-effect, were compared with the

obtained results from measuring the photocurrent spectra.
And then, quantum confined Stark-Effect (QCSE), which is
applicable to the optical modulator, was measured by the
photocurrent.

3-2.Observation of the QW of GaAs on Si

3-2-1.TEM observation

Fig.3-1 shows the transmission electron microscopy
(TEM) pictures of the GaAs/Al0.2Ga0.8As MQW fabricated on a
Si substrate. The width of the wells in (a) and (b) are 20nm
and (c) are 5nm. They were fabricated by atmospheric MOCVD
by two step method without thermal cycle annealings. In a),
there are dislocations crossing the QW. And just in the
region of crossing, the MQW slips out of the line by the
dislocation. In b), windings of the MQW were observed. They
may make the QW properties dull, and lose the steepness of
the light absorption edge. But the slips and windings are
seldom found in the MQW, and usually fine MQW can be
fabricated even in Lz = 5.0 nm. (c) shows the 5 times QWs
that has no slips and windings.

3-2-2.Photo-Luminescence (PL) spectra

We investigated the fluctuation of MQWs on Si substrate
by PL. Fig.3-2 shows the PL spectra of the GaAs/Al0.2Ga0.8As
MQW on Si (a), (b) and undoped GaAs on Si (c) at 4.2K. In
the figure, the MQW sample (a) consists of 40 undoped GaAs
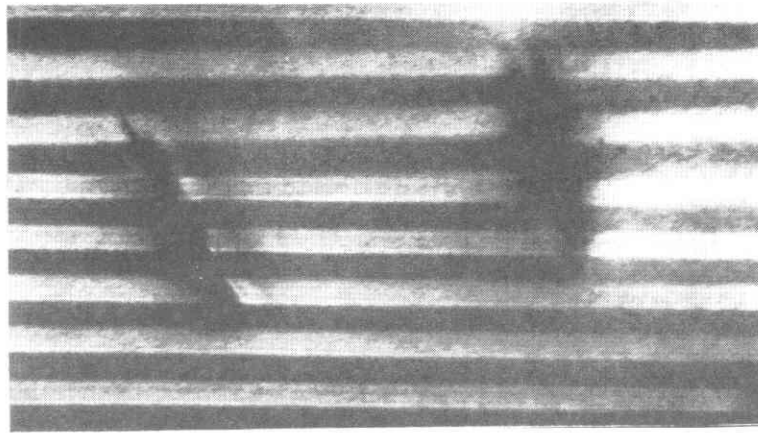
Lz=20nm

a)   100nm
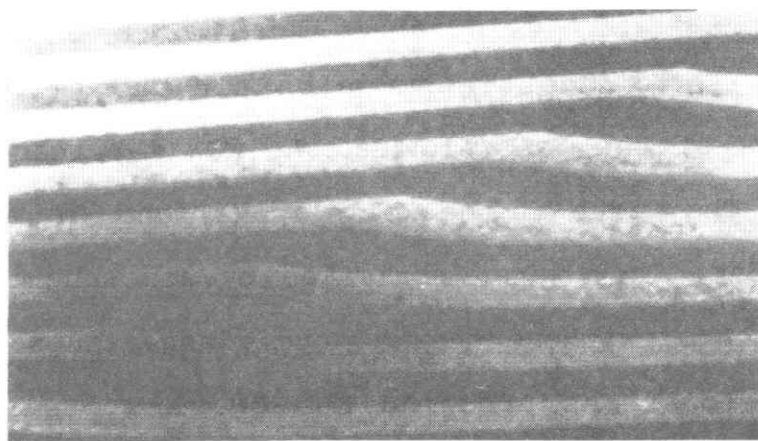
Lz=20nm

b)   100nm
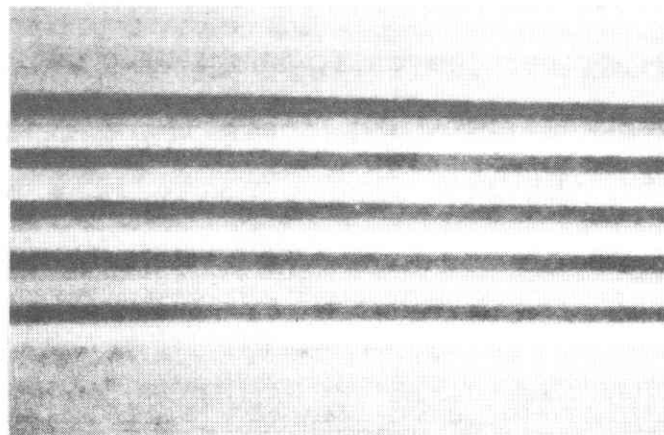
Lz=5nm

c)   50nm

Fig.3-1.TEM pictures of GaAs/Al0.2Ga0.8As MQW.

In a), there are dislocations which make the MQW to slip out of the line. In b), the windings were observed. In C), there are no windings and slips in the QWs.
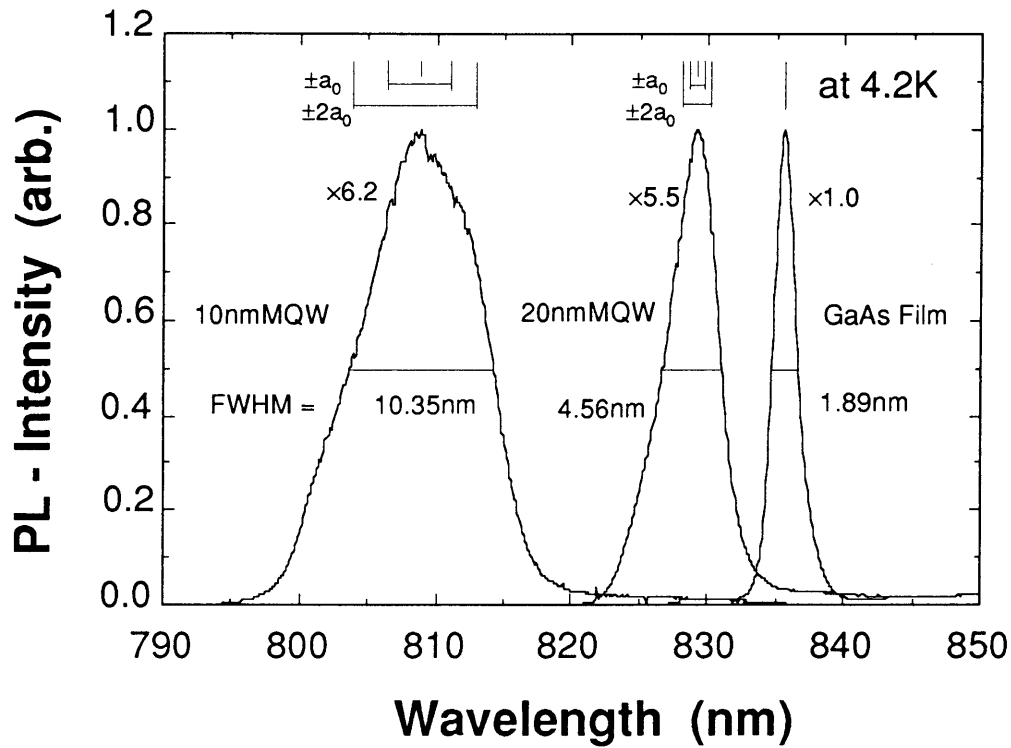
Fig.3-2. PL spectra of the GaAs/Al0.2Ga0.8As MQWs and GaAs film on Si substrate at 4.2K.

a0 is the lattice constant of GaAs (~AlGaAs), and its value is 0.56nm. The fluctuation of the well width (ΔLz) is estimated to be about $\pm$2a0.

wells with thickness (Lz) of 10nm and Al0.2Ga0.8As barriers with thickness (Lb) of 10nm. The sample (b) consists of 20 GaAs wells (Lz=10nm) and Al0.2Ga0.8As barriers (Lb=20nm). All of the samples were fabricated by the atmospheric MOCVD by two step method without thermal cycle annealings.

The full width of half maximum (FWHM) of the spectra of GaAs on Si (sample (c)) is 1.88nm and this value was due to errors of the equipment and imperfections of the GaAs crystal on Si. Because the measurement temperature was very low, the effect from the high energy free carrier was negligible. The FWHM of the samples of (a) and (b) were 10. 35nm and 4.56nm, respectively. Both of the value were conceived to contain the value measured at the sample (c). So the real effects to the PL spectra from the MQW was given to deconvolute the MQW spectra with GaAs spectra. In this case, the effects to the FWHM of the PL spectra of MQW were approximately obtained by deducting the FWHM value of the sample (c). In Fig.3-2, lines in the upper part indicate the peak positions and calculated fluctuations in well size (ΔLz) of $\pm a_0$ and $\pm 2a_0$ to every MQW. The a_0 is the lattice constant of GaAs (a_0=0.56nm). The deducted FWHM value of the sample (c) from those of the sample (a) and (b) shows the effect from ΔLz. This value was found to be about $\pm 2a_0$[11]. It is pretty large for the narrow QW, since it affects strongly as the Lz decreases. But this value also contains the effects from the winding and splitting of the QW (observed by TEM pictures). Such factors affect the quantum levels.

The real fluctuation in well size (ΔLz) must be smaller than $\pm 2a_0$.

3-3. The absorption energy at the room tempetature

3-3-1. Calculation of the electron-hole energy

It is known that GaAs on Si has the biaxial stress due to the difference of the thermal expansion coefficient between Si and GaAs[12)~15)]. Biaxial tension in the QW plane is equivalent to the sum of a hydrostatic tension and uniaxial compression along the growth direction. Hydrostatic tension is known to decrease the band gap of GaAs and uniaxial compression splits the heavy-hole and light-hole exciton. Under the biaxial tension of magnitude X, the shift of the transition energy is given by following equations[12)]:

$$\Delta Ehh = -2AX + BX \qquad\qquad 3\text{-}1.$$
$$\Delta Elh = -2AX - BX \qquad\qquad 3\text{-}2.$$

A is the hydrostatic coefficient and its value is 3.77meV/kbar, while B is the sheer coefficient and its value is 2.69meV/kbar. We can get the transition energy from Eq. 3-1, and also the binding energy between heavy/light-hole and electron exciton in the absence of stress. The quantum level in the symmetric barrier height is obtained by solving the well known equation[16)].

$$\tan(k_2 Lz/2) = m_2{}^* k_1 / m_1{}^* k_2 \qquad\qquad 3\text{-}3.$$

$$K_2 = \sqrt{\frac{2m_2{}^* E}{\hbar}} \qquad\qquad 3\text{-}4.$$

$$K_1 = \sqrt{\frac{2m_1{}^* (V_0 - E)}{\hbar}} \qquad\qquad 3\text{-}5.$$

Here, $m_j{}^*$ (j=1,2) is the effective mass, and V_0 is the barrier height. In this calculation, the Dingle's rule is used for the determination of V_0. And the band to band transition energy of GaAs and Al0.25Ga0.75As at room temperature in no stress conditions are 1.424eV and 1.736eV[17], respectively. The model used for this calculation is the GaAs QW in Al0.25Ga0.75As. In this structure, only n=1 level exists. The calculated results using Eq.3-1 to Eq.3-5 are shown in Fig.3-3. In this figure, "2.3kbar" means the average value of the residual stress in GaAs fabricated on Si at 750°C temperature. Fig.3-3 shows that both electron to heavy-hole energy and electron to light-hole energy are very close to each other at Lz<12nm in 2.3kbar.

3-3-2.Photocurrent spectra measurement

The quantum levels were evaluated by measuring photocurrent[18][19]. The monochromatic light from Ti:sapphire laser was irradiated to the sample's surface. Fig.3-4 shows the schematics of the measuring system. Then the current
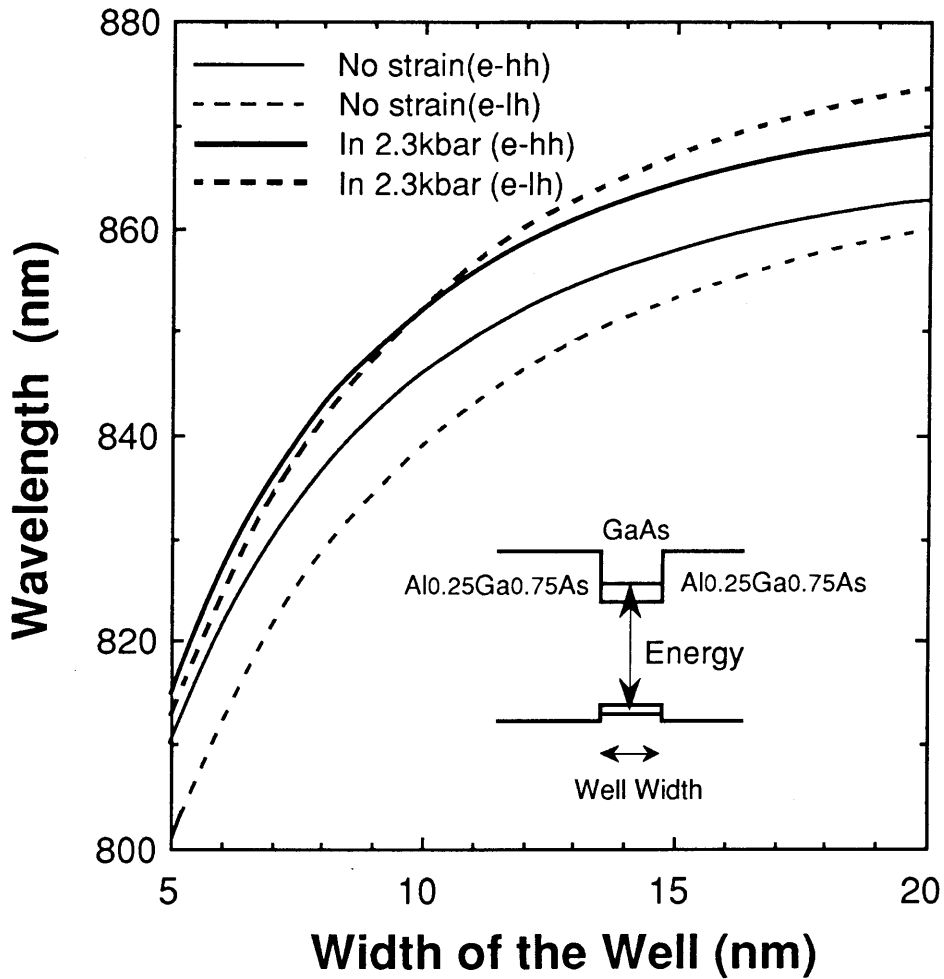
**Fig.3-3.Calculated wavelength corresponding to the
electron-hole exciton energy.**

Solid lines shows e-hh and broken line e-lh. GaAs on
Si have about 2.3kbar biaxial tension in the growth
plane. The energys of e-hh and e-lh are the same
about Lz=10nm in 2.3kbar tension and very close to
each other in Lz<12nm region.
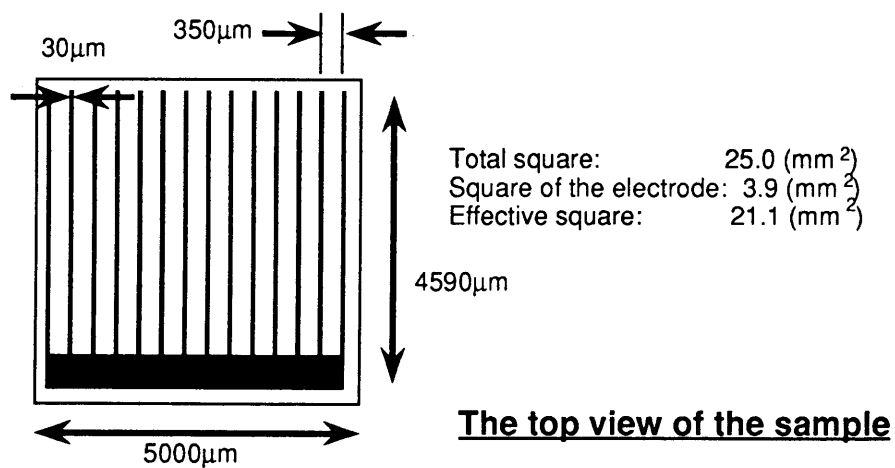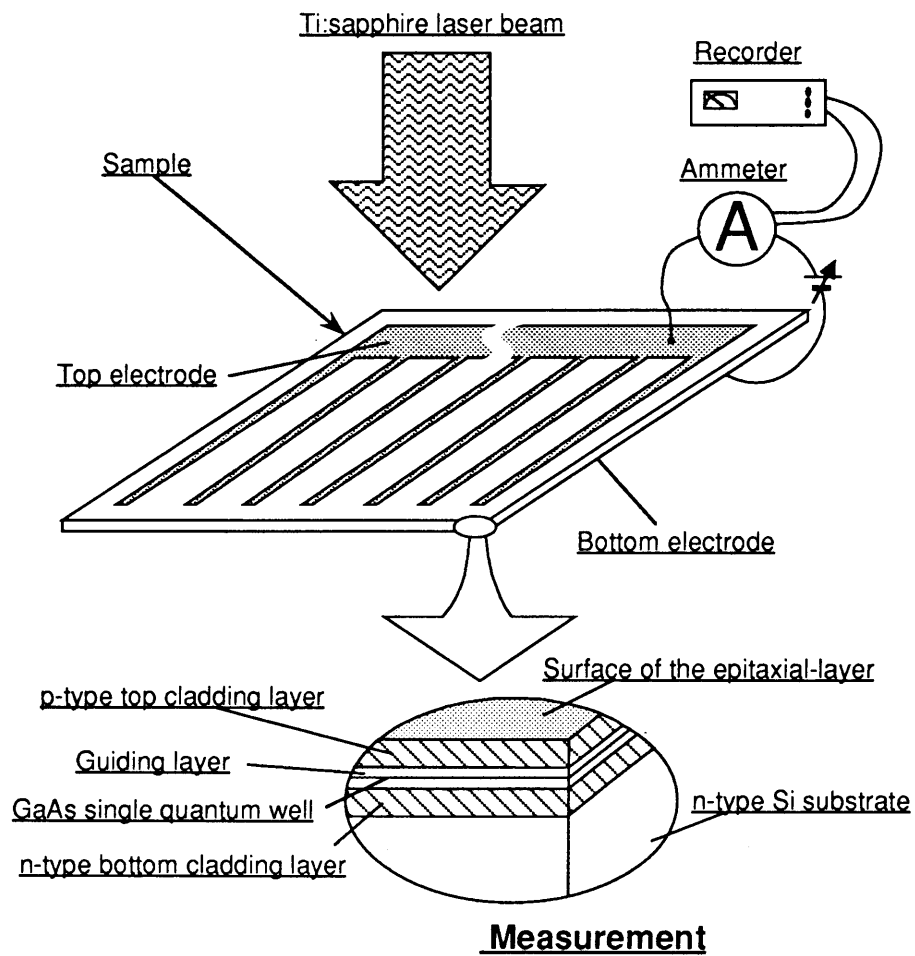
Fig.3-4. Schematics of the sample structure and the measuring system of photocurrent.

(which is generated if the absorption occurred) was measured by an ammeter. In this method, the light absorption of the sample is easily obtained at the room temperature.

All the epi-layers of this sample were grown by MOCVD with radial manifold (which is very convenient for making QWs) using two step method. The growth temperature was 750° C. As a substrate, back-coated (with SiO_2) n-type (100) Si oriented 2° off toward [011] was used (resistivity = $0.02\Omega cm$). A 0.7μm-thick Al0.25Ga0.75As guiding layer with GaAs SQW in the center of the layer was sandwiched between 1.0μm-thick Al0.3Ga0.7As cladding layers. To reduce the dislocations, thermal cycle anealings (from 300°C~850°C) were performed three times during the fabrication of the Al0.3Ga0.7As cladding layer. The top Al0.3Ga0.7As layer was doped with Zn to $p=1\times10^{18}cm^{-3}$ and the lower with Se to $n=1\times10^{18}cm^{-3}$. As gas sources for the dopant, DEZn and SeH2 were used. The Al0.25Ga0.75As layer was undoped. The carrier density of the guiding layer was less than $1\times10^{15}cm^{-3}$ (the conduction type was n-type.). The carrier density in the Al0.25Ga0.75As layer has to be kept as small as possible because the free carrier absorption affects strongly the propagation loss. A p-i-n junction was formed in the sample. The ohmic electrodes were fabricated at the both sides of the sample.

The comparison between the photocurrent from SQW on Si substrate and on GaAs substrate is shown in Fig.3-5. The well width of these two samples were 8.3nm and the
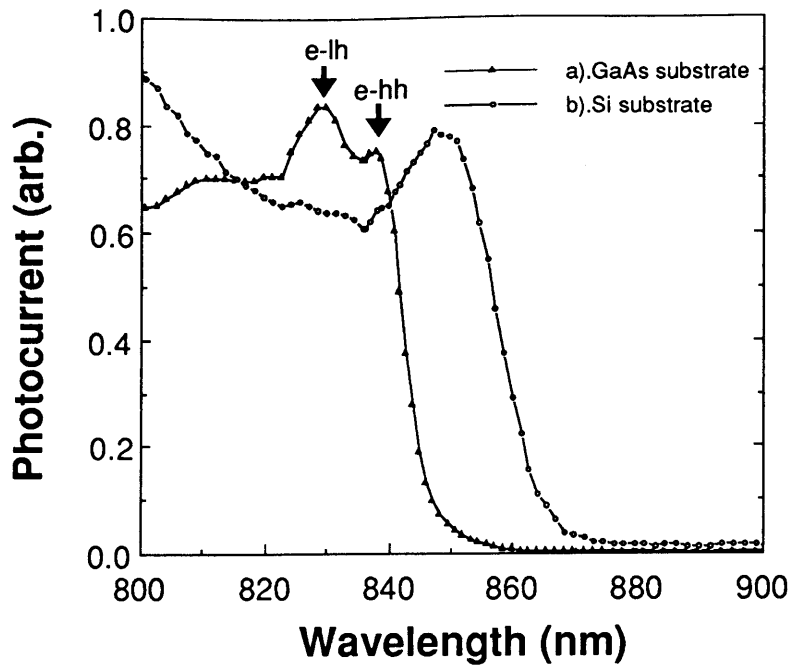
Fig.3-5. Photocurrent spectra of the GaAs/Al$_{0.25}$Ga$_{0.75}$As QW.

(- ▲ -) shows the spectra from the SQW fabricated on GaAs substrate and (- • -) shows that of on Si substrate. The well width (Lz) was 8.3nm in both samples. Two peaks from e-hh and e-lh are recognized in the sample a), but in the sample b), only one peak can be recognized.

structures of both samples were the same except for the substrate. In the case of the GaAs substrate, two peaks clearly appear[20][21] (one is due to the heavy hole and the other is due to the light hole.) and the photocurrent peaks which correspond to the absorption wavelength peak agree well with the calculated results (in the Fig.3-1). On the other hand, in the case of the Si substrate, the heavy hole level and the light hole level are almost the same. So we can recognize only one peak with both heavy hole absorption and light hole absorption contained in it. These results also agree with the calculated ones. The absorption of the QW on Si substrate begins at about a 13.5nm longer wavelength than that of the QW on GaAs.

Fig.3-6 shows the photocurrent spectra obtained by different well widths (4.0, 8.3 and 14.0nm). Fig.3-7 shows the peak wavelength versus the well width, these results agree with the calculated ones. The estimated FWHM of the photocurrent spectra are also shown in Fig.3-7. The narrower well width generates the greater FWHM. This is because the no-uniformity of the well width strongly affects the narrow QW.

3-4.QCSE of GaAs/AlGaAs on Si

3-4-1.Quantum Confined Stark-Effect (QCSE)

By the application of an electric field perpendicular to the QW layers, the square-well potential in QW becomes
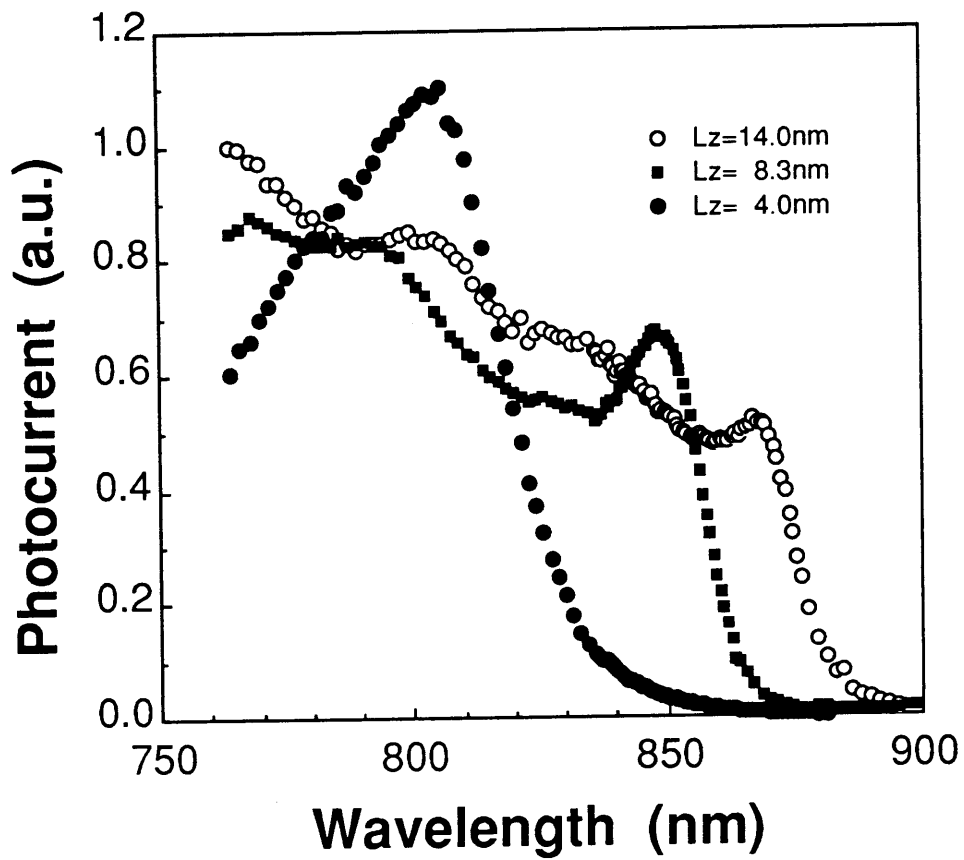
Fig.3-6. The photocurrent from different well widths

(Lz) fabricated on Si substrate.

Every absorption peak contains both e-lh and e-hh

absorptions.
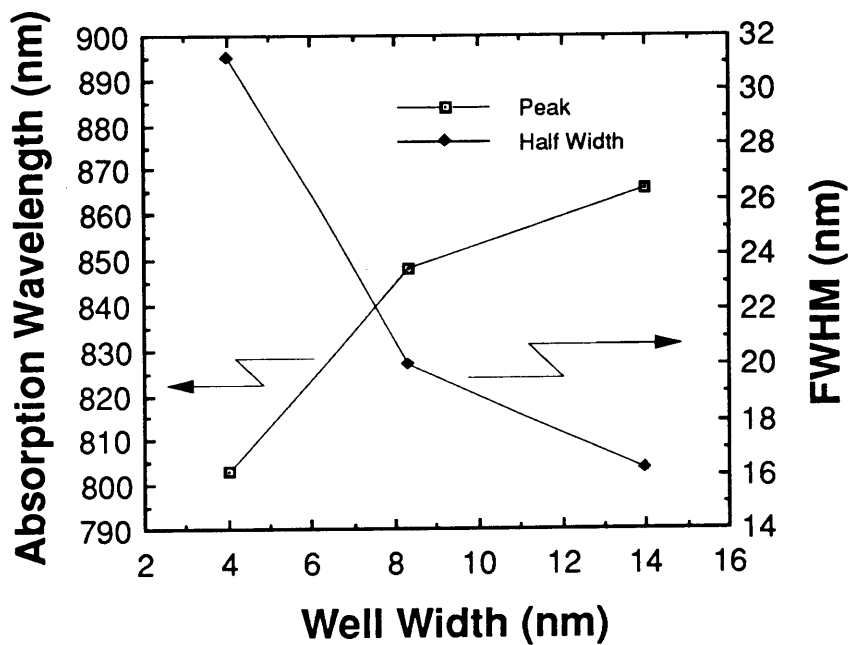
Fig.3-7. Peak wavelength and their half width versus well width .

The wavelength of every peak agree with the calculated one under the consideration of the stress.

inclined. This change brings about the change in absorption

spectra by the following two effects:

1).The change in energy eigenvalue in the QW

2).Separative polarization of the wave function of electrons

and holes.

When the values of the well width (W) and electric field (F)

are small, the theoretical energy shift ΔE in the infinite

quantum well was calculated[22]. They are follows:

$$\Delta E = -C \frac{m^* e^2}{\hbar^2} L_z^4 F^2 \qquad \qquad 3\text{-}6.$$

$$C = \frac{1}{24\pi^2} \left(\frac{15}{\pi^2} - 1 \right)$$

$$eFL_z \ll \frac{\hbar^2}{2m^*} \left(\frac{\pi^2}{L_z} \right) \qquad \qquad 3\text{-}7.$$

As shown in Eq.3-6, the energy shift (ΔE) due to the

application of the electric field is proportional to the

square of the applied field (F) and to the fourth power of

the well width (L_z).

When L_z or F become larger, (when Eq.3-7 can not stand

up) the effect from 2). have to be considered[22]. Detailed

calculations were done by Bastard et al.. In their

calculations, the effective shifts are shown. Such shifts of

the excitonic energy in quantum well due to the electric

field are called the quantum confined Stark-Effect (QCSE)[23]

~[29]. A lot of experimental results are also reported. All of

their results show the clear peak shift due to the electric

field application.

3-4-2.Measurement

The I-V characteristics of the sample are shown in Fig. 3-8. The diffusion potential is about 0.7 V and the breakdown voltage is around 8.2V. The leakage current in the reversed bias is small enough compared with that of the photocurrent. The input light was irradiated parallel to the growth direction. In this method, both the electrical field and magnetic field are perpendicular to the growth direction. The application of the electric field to the sample was done by DC power supply controlling the voltage. The leakage current due to the application of the voltage was subtracted. The effect of the electric field on an excitonic absorption was examined by measuring the photocurrent under reverse bias. The photocurrent is corresponding to the real light absorption spectrum. The measurement systems of the QCSE are the same as shown in Fig.3-4.

3-4-3. Obtained properties

The obtained results from the photocurrent as a function of the wavelength of the incident light are shown in Fig.3-9 and Fig.3-10.[30]. Fig.3-9 is about the QW on Si substrate and Fig.3-10, GaAs substrate. The structure and the growth condition of epi-layer in both two samples were the same ($Lz=8.3nm$).
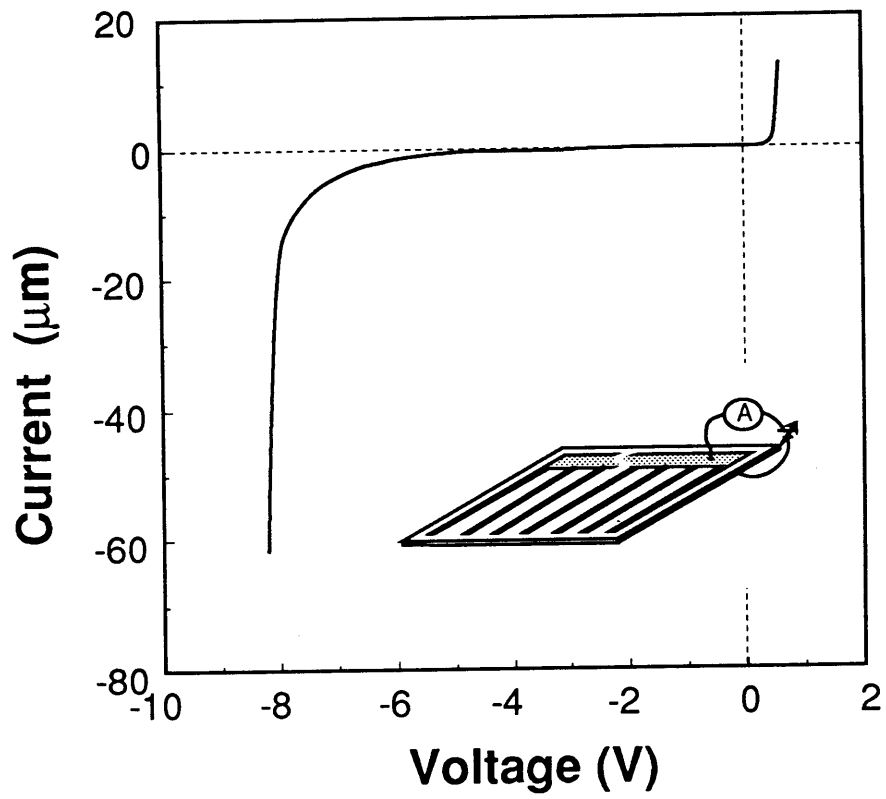
Fig.3-8. The I-V characteristics of the sample.
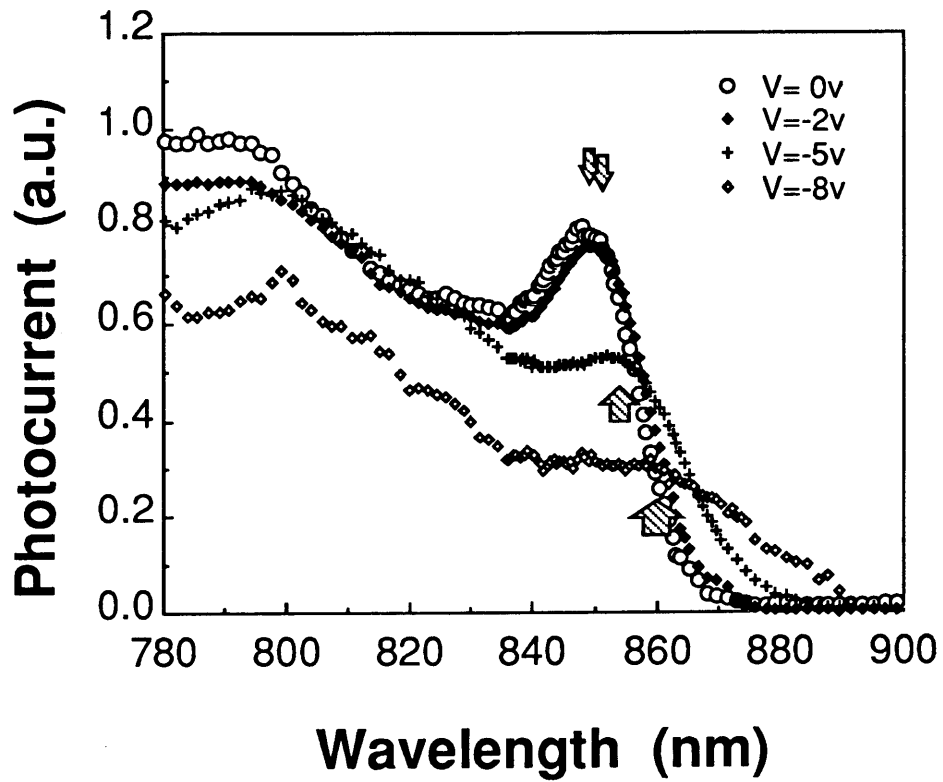
Fig.3-9. The shift of the photocurrent spectra by the QW in the different bias application.

This sample was fabricated on Si substrate. Arrows show the observed peak position.
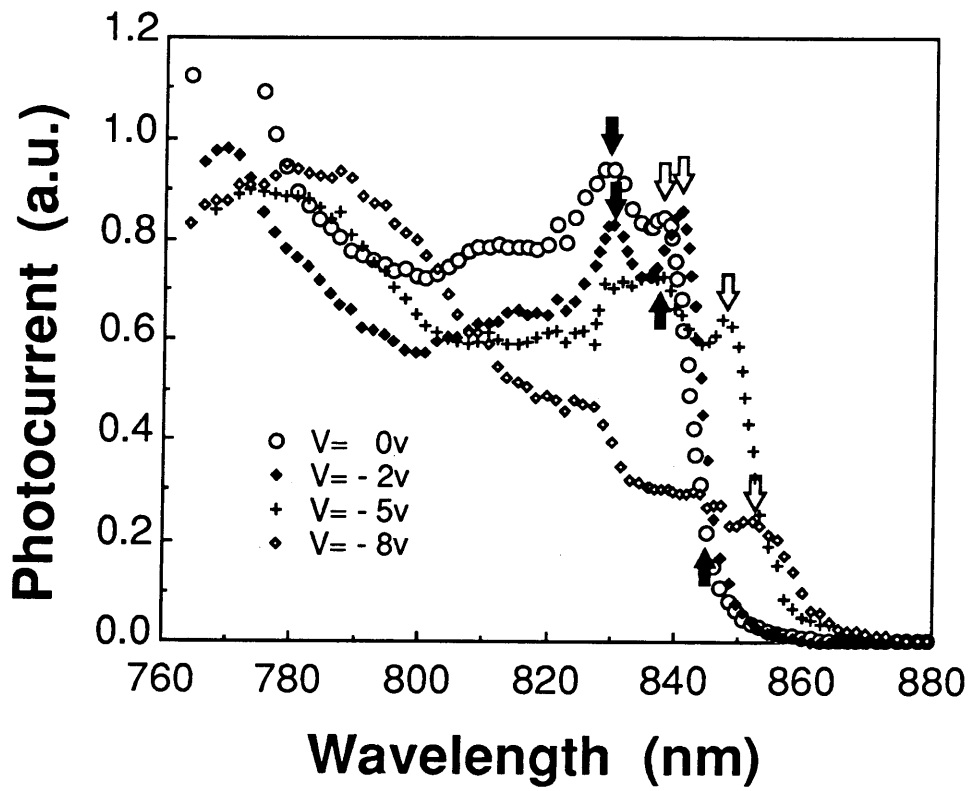
Fig.3-10. The shift of the photocurrent spectra by the QW in the different bias application.

This sample was fabricated on GaAs substrate. The black arrows show the e-lh absorption and white arrows show the e-hh absorption.

In Fig.3-10, two peaks can be recognized near the absorption edge. The wavelength of the peaks agree well with the results of the calculation. One (white arrow) is due to heavy hole exciton, the other (black arrow) due to light hole exciton. Both peaks were shifted to a longer wavelength. And broadened as the applied voltage increased. This behavior shows the obvious QCSE characteristics reported by D.A.B.Miller et al.

In Fig.3-9, The observed peaks are indicated by arrows. In this figure, the peaks of both heavy hole and light hole are not confirmed. Only one peak appears. It is because the peaks of both heavy hole exciton and light hole exciton are very close to each other in the case of the Si substrate. From the result of T.H.Wood et al., the peak shift by the electric field was more pronounced for heavy hole exciton than light hole exciton. But the relative shift of the absorption edge can be observed as the applied voltage increases. Fig.3-11 shows the drift of peaks versus the applied electric field. The length of the mark (vertical direction) shows the estimated halfwidth of the peak.

3-5.Conclusion

The characteristics of GaAs/AlGaAs QW on Si substrate fabricated by MOCVD were studied.

First, the TEM pictures and PL spectra of the MQW were investigated. In the TEM pictures, there were some windings
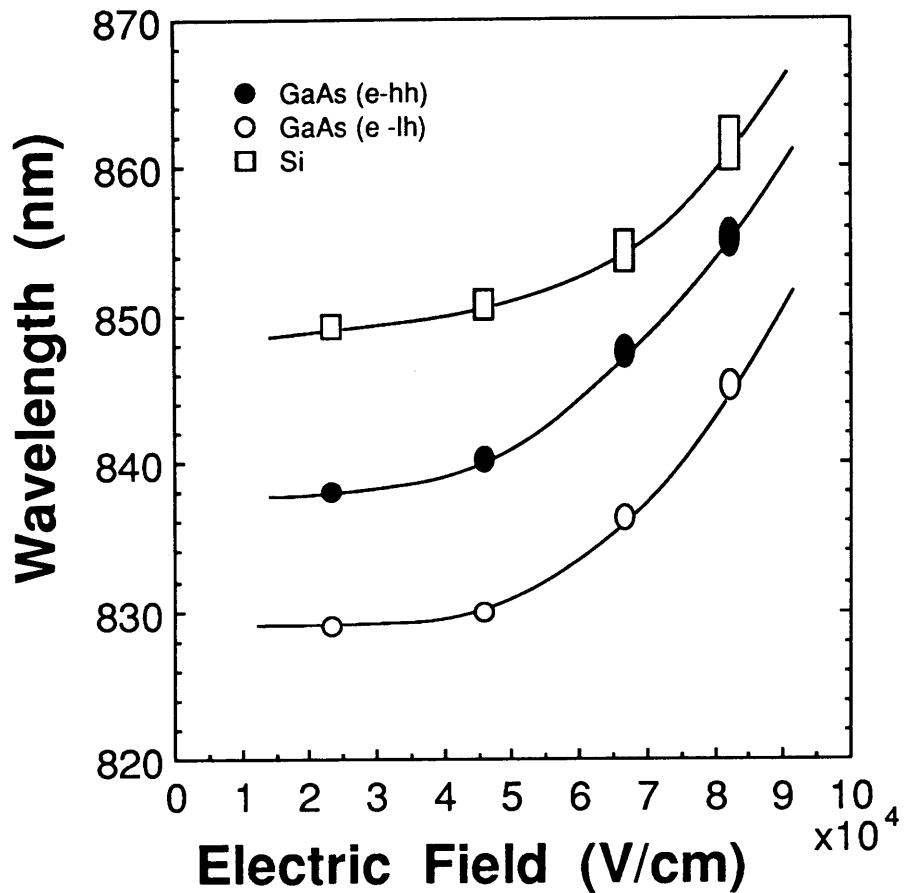
Fig.3-11.The shift of the electron-hole absorption

wavelength.

● indicates e-hh

○ indicates e-lh in QW fabricated on GaAs

substrate

□ indicates the peak observed in QW

fabricated on Si substrate.

The length of the mark (vertical direction) shows

the estimated peak position.

and splittings in the MQW. And they seemed to be originated from the dislocations. And from PL spectra, the fluctuation in well size in MQW was estimated. If the width of the PL spectra is generated only by the effect from ΔLz, the estimated ΔLz equals to $\pm 2a_0$. But practically, ΔLz must be smaller than $\pm 2a_0$ considering the winding and splitting effects of the MQW that were observed by TEM.

Then, the electron-hole energy of GaAs/Al0.25Ga0.75As QW was calculated under the consideration of the effect from the stress. This calculation shows that both electron to heavy-hole energy and electron to light-hole one are very close to each other at $Lz<12$nm, and these two energies become the same at $Lz=9.6$nm on Si substrate. And to make sure if the calculation is correct, the light absorption edge of the QW samples were evaluated by measuring the photocurrent in room temperature. The absorption edge of the same QW structure (GaAs/Al0.25Ga0.75As) on Si substrate and on GaAs one were compared with each other. About 10nm difference of the absorption edge was observed and this value was almost the same as the calculated one considering the effect of the stress. And the absorption edge of different well width on Si substrate were measured. They agreed well with the calculated values. These results show that absorption level of the QW on Si substrate can be easily obtained by the calculation with considering the effect from stress.

And then, the QCSE on Si substrate was measured. The

sample with p-n junction and a 8.3nm SQW showed a large shift of the absorption edge as the applied voltage increased. And the shift was almost the same as the same structural sample fabricated on a GaAs substrate. These results show that the GaAs on Si can be applied to quantum devices utilizing QCSE in practical use.

References

1) H.M.Gibbs, S.S.Tarng, J.L.Jewell, D.A.Weinbergar, K.Tai, A.C.Gossard, S.L.McCall,A.Passner and W.Wiegmann:Appl. Phys.Lett.,41, (1982),221.

2) T.Venkatesan, B.Wilkens, Y.H.Lee, M.Warren, G.Olbright, H.M.Gibbs, N.Peyghambarian, J.S.Smith and A.Yariv:Appl. Phys.Lett.,48, (1986),145.

3) T.H.Wood, C.A.Jr.,Burrus, D.A.B.Miller, D.S.Chemla, T.C. Damen, A.C.Gossard and W.Wiegmann:Appl.Phys.Lett.,44, (1984),16.

4) T.H.Wood, C.A.Jr.,Burrus, D.A.B.Miller, D.S.Chemla, T.C. Damen, A.C.Gossard and W.Wiegmann:IEEE.J.Quantum Electron.,QE-21, (1985),117.

5) G.D.Boyd, D.A.B.Miller, D.S.Chmla, S.L.McCall, A.C., Gossard and J.H.English:Appl.Phys.Lett.,50, (1987),1119.

6) K.B.Nichols, B.E.Burke, B.F.Aull, W.D.Goodhue, B.F. Gramatoff, C.D.Hoyt and A.Ver:Appl.Phys.Lett.,52, (1988),1116.

7) D.A.B.Miller, D.S.Chmla, T.C.Damen, A.C.Gossard, W.Wiegmann, T.H.Wood and C.A.Jr.,Burrus:Appl.Phys. Lett.,45,(1984),13.

8) D.A.B.Miller, D.S.Chmla, T.C.Damen, T.H.Wood, C.A.Jr., Gossard and W.Wiegmann:IEEE.J.Quantum Electron.,QE-21, (1985),1462.

9) D.A.B.Miller, J.E.Henry, A.C.Gossard and J.H.English: Appl.Phys.Lett.,49, (1986),821.

10) N.Wada, S.Sakai, Y.Ueta, S.Koshiba, K.Uematsu, K. Higashiyama, Y.Shintani, T.Yuasa and M.Umeno:Jpn.J. Appl.Phys.,30, (1991),L396.

11) L.Goldstein, Y.Horikoshi, S.Tarucha and H.Okamoto:Jpn.J. Appl.Phys.,22, (1983),1489.

12) C.P.Kuo, S.K.Vong, R.M.Cohen and G.B.Stringfellow:J. Appl.Phys.,57, (1985),5428.

13) C.Jagannath, S.Zeman, P.Norris and B.S.Elman:Appl.Phys. Lett.,51, (1987),1268.

14) M.Chandrasekhar and F.H.Pollak:Phys.Rev.,B15, (1977), 2127.

15) C.Jagannath, Emil.S.Koteles, Johnson.Lee, Y.I.Chen, B.S. Elman and J.Y.Chi:Phys.Rev.,B34, (1986),7027.

16) O.Hiroshi:Supperlattice and Quantum Well for Optelectronics:CORONA PUBLISHING CO.,LTD, (1988),7.

17) B.Moonemar, K.K.Shih and G.D.Pettit:J.Appl.Phys.,47, (1976),2604.

18) T.Miyazawa, S.Tarucha, Y.Suzuki and H.Okamoto:Jpn.J. Appl.Phys.,25, (1988),L200.

19) K.Wakita, Y.Kawamura, Y.Yoshikuni, H.Asahi ane S.Uehara: IEEE J.Quantum Electron.,QE-22, (1986),1832.

20) S.W.Kirchoefer, N.Holonyak,Jr., K.Hess, D.A.Gulino, H.G. Drickamer, J.J.C.leman and P.D.Dapkus:Appl.Phys.Lett., 49, (1982),821.

21) D.A.B.miller, D.S.Chemla, J.J.Elenberger, P.W.Smith, A. C.Gossard and W.T.Tsang:Appl.Phys.Lett.,41, (1982),679.

22) G.Bastard, E.E.Mendez, L.L.Chang and L.Esaki:Phys.Rev.,

B28, (1983),3241.

23) T.H.Wood, C.A.Burrus, D.A.B.Miller, D.S.Chemla,J.C.
Damen, A.C.Gossard and W.Wiegmann:Appl.Phys.Lett.,44,
(1984),16.

24) D.A.B.Miller, D.S.Chemla, J.C.Damen, A.C.Gossard and W.
Wiegmann, T.H.Wood, C.A.Burrus:Appl.Phys.Lett.,45,
(1984),13.

25) D.A.B.Miller, D.S.Chemla, J.C.Damen, A.C.Gossard and W.
Wiegmann, T.H.Wood, C.A.Burrus:Phys.Rev.Lett.,53,
(1984),2173.

26) J.A.Brum and G.Bastard:Phys.Rev.B31, (1985),3893.

27) D.A.B.Miller, D.S.Chemla, T.C.Damen, T.H.Wood, C.A.
Burrus, A.C.Gossard and W.Wiegmann:IEEE.J.Quantum
Electron.QE-21, (1985),1462.

28) D.A.B.Miller, D.S.Chemla,J.C.Damen, A.C.Gossard and W.
Wiegmann, T.H.Wood, C.A.Burrus:Phys.Rev.B32, (1985),
1043.

29) J.S.Weiner, D.A.B.Miller, D.S.Chemla, T.C.Damen, C.A.
Burrus, T.H.Wood, A.C.Gossard and W.Wiegmann:Appl.Phys.
Lett.,47, (1985),1148.

30) T.Yuasa, M.Umeno, Y.Nagashima, K.Arimochi and T.Jimbo:
to be published in Proc. of ICPS-21, Beijing.